ANL-7542

Argonne National Laboratory

A CATALOG OF ROD-DROP AND TRANSFER-FUNCTION DATA FROM EBR-II RUNS 25 THROUGH 30A

by

I. A. Engen and R. W. Hyndman

Printed in the United States of America
Available from
National Technical Information Service
U.S. Department of Commerce
Springfield, Virginia 22151
Price: Printed Copy $3.00; Microfiche $0.65

ANL-7542
Reactor Technology

ARGONNE NATIONAL LABORATORY
9700 South Cass Avenue
Argonne, Illinois 60439

A CATALOG OF ROD-DROP AND TRANSFER-FUNCTION DATA FROM EBR-II RUNS 25 THROUGH 30A

by

I. A. Engen and R. W. Hyndman

EBR-II Project

May 1970

TABLE OF CONTENTS

LIST OF FIGURES

LIST OF FIGURES

LIST OF TABLES

A CATALOG OF ROD-DROP AND TRANSFER-FUNCTION DATA FROM EBR-II RUNS 25 THROUGH 30A

by

I. A. Engen and R. W. Hyndman

ABSTRACT

Reactivity-perturbation experiments have been conducted in EBR-II during many reactor runs. The results of the experiments conducted during runs 25 through 30A are presented here to provide a large amount of data in a compact form suitable for reference. This report discusses the experimental rod-drop and oscillator methods used, but does not discuss the application of the results to reactor evaluation.

I. INTRODUCTION

Kinetics studies of Experimental Breeder Reactor II (EBR-II) were made during runs 25 through 30A to study the stability characteristics of the reactor, enable mathematical modeling, and determine the effects of interchange of depleted-uranium blanket with stainless steel reflector. The present report describes the methods used and gives the results in tabulated and graphic form.

These results were obtained largely by the rod-drop method, but include oscillator-rod measurements from run 26. Kinetics studies of EBR-II have been hampered by mechanical failures of the oscillator rod. The original reciprocating oscillator failed during the initial power runs, requiring the development of the rod-drop technique. Rod-drop measurements were begun in run 24. During the same run, a new rotary oscillator was installed and checked out. The oscillator data were initially collected by the analog Fourier technique, but an evaluation of the technique indicated that the system error was approximately ±4%. To reduce the error and speed up analysis, an on-line digital method was developed.[1] The experimental checkout, at a reactor power level of 500 kW, showed the difference between calculated and measured values of the transfer function to be only 0.25% in amplitude and 0.25° in phase. The usefulness of the oscillator proved to be limited, however, because the rotating section through the reactor rubbed against the thimble at 30 MW and above. This could only be caused by bowing of either the rotating section or the thimble. The

oscillator was removed and the rod-drop method resumed. Rod drops were used for analysis for runs 25 through 30. A new oscillator system was installed for run 26. Again the rubbing occurred and only limited data were obtained.

Although the kinetics studies have been hampered by lack of the oscillator, much valuable data have been obtained from rod drops. The rod-drop technique consists of (a) data acquisition, using the IBM 1620 computer in real time, (b) performance of an inverse kinetics computation to obtain the feedback reactivity, and (c) development of a describing function for the feedback reactivity.

The following sections describe the oscillator and rod-drop methods in detail, and then describe the data-reduction methods used.

II. MEASUREMENT SYSTEM

A. Oscillator Method

Transfer-function data for runs 24 and 26 were based on a sinusoidal excitation of reactor power with a rotary-type oscillator rod located in a control-rod position. The drive mechanism for the rod consisted of a synchronous motor that drove through a Vari-Speed gearbox to provide a reactivity-insertion rate ranging from 0.002 to 9 rps. The upper limit of 9 rps, established through out-of-pile tests, was due to mechanical resonance effects in the drive rod that coupled the Vari-Speed drive to the oscillator rod. The lower limit of 0.002 rps was fixed by mechanical limitations of the gear train.

Sine and cosine potentiometers were attached directly to the Vari-Speed unit so that one complete rotation of the oscillator rod resulted in complete sine and cosine cycles. Although attempts were made to minimize the angular displacement of the sine-cosine signals with respect to the reactivity insertion, the exact relationship was established during zero-power tests by rotating the oscillator rod in both directions.

Figure 1 is a cross-sectional view through the oscillator rods used during runs 24 and 26. Rotation of the rods about the vertical axis cycled the B_4C column(s) in and out with respect to the core.

For run 24, the oscillator rod contained two columns of B_4C, which were counterbalanced by two columns of Al_2O_3. Both materials were contained in Type 304 stainless steel tubes. The total reactivity worth of the rod measured between the least and the most reactive positions was established as 21.8 Ih through period measurements at essentially zero power.

Although useful information was generated with this rod in run 24, two deficiencies were noted. The amplitude of the reactivity insertion was too large; unacceptably large power oscillations were generated at the lower frequencies. Even more objectionable was a tendency for the rod to rub against its thimble at the lower frequencies and, on occasion, to seize. The rubbing tendency was dependent not only on frequency but on power. Thus, at higher power levels, the rod was very likely to rub and seize at lower frequencies. These effects were attributed to the unequal generation of heat in the poison and inert sections. The resulting temperature gradient presumably caused enough bowing in either the rod or its thimble to bring about a mechanical contact.

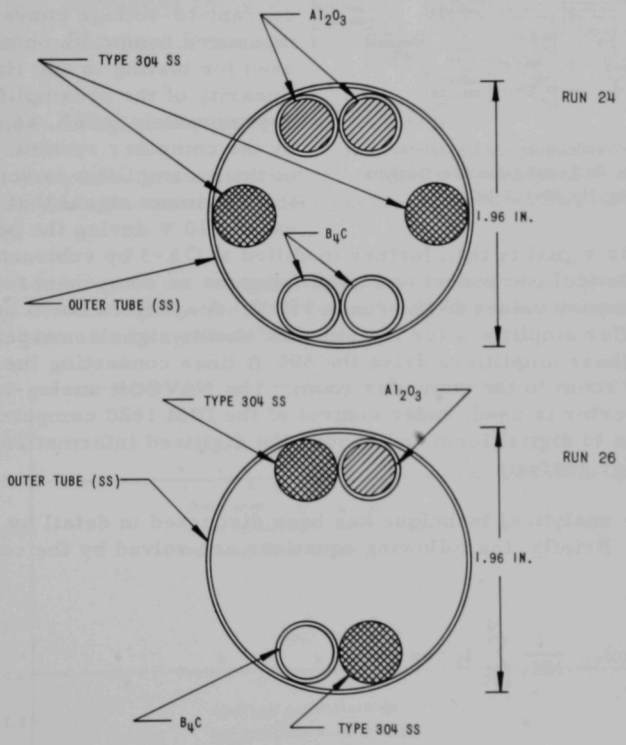

Fig. 1. Cross Sections of Rotating Oscillator Rods Used in Runs 24 and 26

In an attempt to eliminate these undesirable effects, a second oscillator rod was fabricated. In this second rod, one of the two poison sections was replaced with a solid Type 304 stainless steel rod. Counterweights on the opposite side consisted of a stainless steel rod and a tube filled with Al_2O_3. Subsequent period calibration measurements, conducted between the least and most reactive positions, resulted in a peak-to-peak reactivity worth of about 11 Ih.

Despite the efforts to reduce the temperature gradient across the rod by removing approximately half the heat-generating source, i.e., the B_4C poison, subsequent tests revealed that the rubbing persisted. Nevertheless, useful information at the higher frequencies was obtained during run 26 with the second oscillator rod.

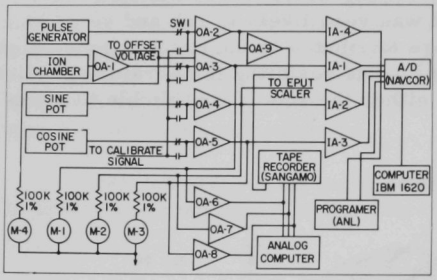

Fig. 2. Signal-conditioning and Digital-reduction Systems for Transfer-function Analysis. ANL Neg. No. ID-103-I5335.

Figure 2 is a diagram of the signal-conditioning and digital-reduction systems for transfer-function analysis. The ion-chamber preamplifier (OA-1) is a standard operational amplifier used as a current-to-voltage converter. The measured bandwidth on all ranges used for testing is 480 Hz. The linearity of the preamplifier is approximately 0.02%, as measured by the computer system. The output of the preamplifier is set to obtain the maximum signal that will not exceed 10 V during the peak of the swing. This signal is then further modified at OA-3 by subtracting out the steady-state (dc) component and amplifying the ac component to again keep the peak-to-peak values in the range ±10 V. Amplifiers OA-4 and -5 are used as buffer amplifiers for the sine and cosine signals, respectively. The outputs of these amplifiers drive the 500-ft lines connecting the data-acquisition room to the computer room. The NAVCOR analog-to-digital (A/D) converter is used, under control of the IBM 1620 computer, to convert signals to digital form and to load the digitized information into the computer for analysis.

The analytical technique has been discussed in detail by Hyndman and Tuck.[1] Briefly, the following equations are solved by the computer in real time:

$$\mathrm{Re}(\omega) = \frac{1}{NK_1} \sum_{i=0}^{N} I_i \cos(\omega \Delta t) \qquad (1)$$

and

$$\mathrm{Im}(\omega) = \frac{1}{NK_2} \sum_{i=0}^{N} I_i \sin(\omega \Delta t), \qquad (2)$$

where

N = number of sample points ($N > 2400$) such that sampling is over an integral number of cycles,

I_i = ith sample of ion-chamber output,

Δt = time between samples,

K_1 and K_2 = normalizing constants determined by sampling interval, offset voltage, system gain, and total delayed-neutron fraction,

ω = oscillating frequency,

$Re(\omega)$ = real part of transfer function,

and

$Im(\omega)$ = imaginary part of transfer function.

The computer then prints out the magnitude and phase of the transfer function G(s), the zero-power transfer function $G_0(s)$, and the feedback function H(s).

The accuracy of the transfer-function method is illustrated graphically in Fig. 3, which gives the difference between measured and calculated zero-power phase and amplitude values.

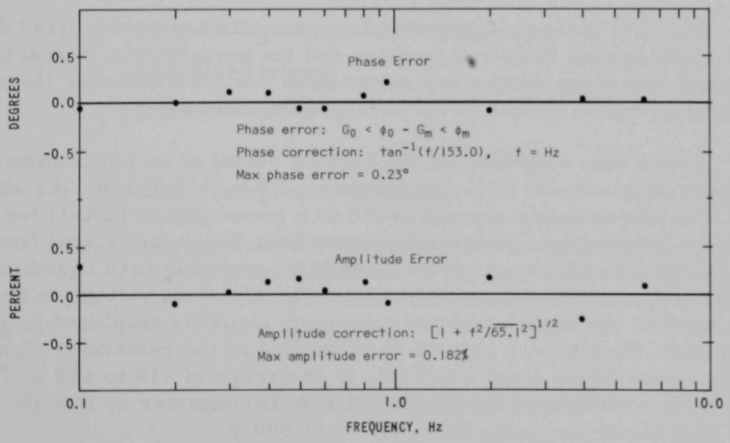

Fig. 3. Accuracy of Open-loop Transfer-function Measurement

B. Rod-drop Method

In the rod-drop method, reactivity is removed in approximately 280 msec from the system in a pseudoramp manner by dropping (scramming)

a control-rod subassembly that contains stainless steel rods in place of fuel elements. Substitution of stainless steel for fuel reduces the total worth of the rod from a nominal value of 130 Ih to approximately 12 Ih. Depending on details of core loading, on type of reflector, and on rod-bank configuration, the worth of the rod varies within the limits ±2 Ih. Because of the variation, the rod is carefully calibrated prior to a series of measurements. Rod drops are controlled from a special panel, which, through supervisory and administrative control, permits the removal of the drop rod from the safety circuits. The rod can then be dropped at the option of the experimenter.

The data-acquisition system used for rod-drop analysis is essentially the same as that used for oscillator-rod experiments, except that the sine and cosine channels are used for the rod-position and experiment-initiate signals. The A/D converter is placed in the digitizing mode by the IBM 1620 computer. Digitizing continues until the test is terminated by the computer. The storage of data starts upon receipt of an initiate signal, 0.5 sec before drop time. The first 0.5 sec of data provides a measure of the average power level before the rod drop. Data are loaded into the computer until any preselected number of data points less than 9000 are stored. After completion of the digitizing and storage, the data are written on magnetic tape for future processing. The sampling rate is determined by an oscillator internally connected to the A/D converter. The maximum sampling rate in this mode of operation is approximately 300 samples per second per channel.

The data stored on magnetic tape consist of nonnormalized digital values representing drop-rod position and the perturbation in reactor power. To explain how these values are normalized, we must examine the signal conditioning, which occurs in the data-acquisition system.

Power data originate as the current output of an ion chamber. The current is proportional to reactor power, $\sim 1.0 \times 10^{-5}$ A/MW. As shown in Fig. 2, the ion-chamber current is fed to a preamplifier (OA-1) for current-to-voltage conversion. Range selection allows the output signal from OA-1 to be confined to the range of 2-8 V, and this signal in turn is fed to a variable-gain operational amplifier (OA-3). An offset voltage is used to delete most of the signal, and the remaining signal is amplified by gain adjustment. Typically, a gain of 30 is applied to the remaining signal so that the output signal from OA-3 lies in the range of -10 to +10 V; the signal is then attenuated by the NAVCOR A/D converter so that the stored power data lie in the range of -1.800 to +1.800 V.

The power trace is reconstructed by measuring the system gain between OA-3 and the computer. The product of the system gain and the offset voltage at OA-3 is added to each stored power point. Power data are next normalized to an average of 24 points that precede the rod drop. Rod position is normalized by referring the total change in signal to the total change in rod position.

This method of data acquisition is used for all rod drops. At zero power (500 kW or less), the rod worth versus position is determined. The resulting rod-worth curve then serves as input for the analysis of rod-drop data taken with the reactor operating at power.

The reactivity calculation is based on an inverse-kinetics code developed by Hyndman and Nicholson.[2] The input to the code consists of the normalized power trace and the rod position. For zero power or calibration, the reactivity is computed and printed out for each position of the rod. Input for the power runs consists of normalized power, rod position, and the rod-calibration curve. The output for the power run is the reactivity feedback versus time.

The reactivity feedback is then used to determine a feedback model by the following equation:

$$FB(t) = \sum_i \frac{A_i \exp(T_i/\tau_i)}{\tau_i} \int_0^{t-T_i} [1 - P(t')] \exp\left(-\frac{t-t'}{\tau_i}\right) dt', \qquad (3)$$

where

$FB(t)$ = feedback,

A_i = magnitude of feedback of ith term,

τ_i = time constant of feedback of ith term,

T_i = transport lag of feedback of ith term,

$P(t')$ = normalized power,

t = time after rod drop,

and

t' = dummy integration variable.

Errors in the instrumentation have been discussed in Section A above. However, one additional source of error is the rod-worth variation as a function of power. As discussed in Ref. 2, a correction must be made for some power levels.

III. EBR-II KINETICS DATA

Reactor-kinetics experiments performed during runs 25 through 30A consisted of oscillator experiments (runs 26B and 26C) and rod-drop experiments during the various runs and subruns itemized in Table I.[3]

TABLE I. EBR-II Core Loadings

Date	Run	Total Number of Subassemblies in Core	Number of In-core Experimental Subassemblies
6/29 to 8/18/67	25C-25E	88	11
9/22 to 9/29/67	26A	88	11
10/11 to 11/20/67	26B	91	12
11/22 to 12/12/67[a]	26C	91	16
3/7 to 3/11/68	27C	90	17
5/9 to 5/13/68	28A	86	6
5/15 to 5/27/68	28B	88	10
5/29 to 6/15/68	28C	88	16
6/26 to 7/5/68	29A	87	15
7/15 to 7/22/68	29C	90	15
8/21 to 9/5/68	30A	91	16

[a]Oscillator experiments but no rod drops during run 26C.

In addition to experimental subassemblies, the core in runs 26B through 28C contained both the oscillator and the stainless steel drop rods. At the end of run 28C, the oscillator was replaced by a standard control rod. A stainless steel inner reflector was used from runs 25 through 29B, after which the stainless steel reflector was replaced by a depleted-uranium blanket.

A. Reduction of Oscillator Data

The data obtained during the oscillator experiments of runs 26B and 26C consisted of transfer-function measurements at 500 kW, 22.5 MWt, 30 MWt, and 41.5 MWt. From these measurements the feedback was calculated.

With the reactor considered to be a linear system, the simple block diagram shown in Fig. 4 represents the relationship of feedback to transfer function,

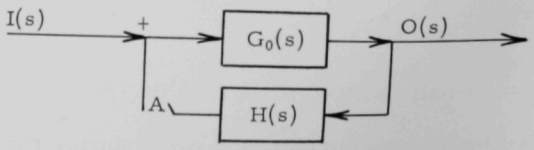

Fig. 4. Block Diagram of Feedback Control System

where

$I(s)$ = driving function,

$O(s)$ = output,

$H(s)$ = feedback,

$G_0(s)$ = open-loop transfer function,

A = switch,

and

s = Laplace-transform variable, $j\omega$.

The open-loop or zero-power transfer function, $G_0(s)$, is determined by the nuclear properties of the reactor core and describes the reactor transfer function for the special case in which the temperature-dependent feedback is negligible. In Fig. 4, this is equivalent to having the switch at A open so that the feedback, $H(s)$, is disconnected. With the switch closed, the feedback is connected and the block diagram represents the closed-loop reactor system operating at some significant power level.

The closed-loop transfer function, $G(s)$, is then defined in terms of the block diagram as

$$G(s) = \frac{G_0(s)}{1 + G_0(s)H(s)}. \tag{4}$$

The feedback $H(s)$ can readily be separated from this expression:

$$H(s) = G(s)^{-1} - G_0(s)^{-1}. \tag{5}$$

Computation of values for $H(s)$ requires $G_0(s)^{-1}$ to be computed. $G_0(s)$ is obtained from the usual space-independent, one-energy-group, linearized reactor-kinetics equations,[4] using six beta fractions as listed in Table II. The equation for the open-loop transfer function is

$$G_0(s) = \frac{n_0}{s\left[\ell^* + \sum_{i=1}^{6} \frac{\beta_i}{s + \lambda_i}\right]},$$

where

n_0 = initial neutron concentration,

β_i = ith delayed neutron fraction,

λ_i = ith decay constant,

ℓ^* = neutron generation time,

and

s = Laplace-transform variable, $j\omega$.

TABLE II. EBR-II Delayed-neutron Parameters

(one-energy group)

Index, i	Delayed-neutron Fraction, β_i	Time Constant, λ_i, sec^{-1}	Index, i	Delayed-neutron Fraction, β_i	Time Constant, λ_i, sec^{-1}
1	0.00025842	0.0127	4	0.00300787	0.3110
2	0.00151386	0.0317	5	0.00104661	1.4000
3	0.00137510	0.1150	6	0.00024178	3.8700

$\beta = \sum_{i=1}^{6} \beta_i = 0.00744364$; $\ell^* = 1.5555 \times 10^{-7}$.

Values for $G_0(s)$, G(s), and H(s) are given in Tables IV through XVII (in Appendix A). Figures 5-10 (in Appendix B) are Nyquist plots of feedback; the units are cents, obtained by multiplying H(s) by $(\beta^{-1} \times 10^2)$.

B. Reduction of Rod-drop Data

Rod-drop measurements resulted in a large amount of data during the period covered. Normalized power and negative feedback as functions of time are shown in Figs. 11-51 (also in Appendix B). The data are smoothed by six-point averaging. It has been noted in Ref. 2 that an adjustment to the rod-worth calibration was necessary for run 26. These values and subsequent adjustments are listed in Table III. The lack of an entry indicates that no adjustment was made. Adjustment consisted of increasing the worth of the rod by a percentage of its calibrated worth.

TABLE III. Rod-worth Corrections (%)

Run Number:	26	27A	27C	28A	28B	28C	29A	29C	30A
Rod Worth, $:	0.04172	0.038		0.0434	0.04923	0.04865	0.04948	0.04075	0.03750
MW/% Flow									
22.5/100	+1			+5		+7			
22.5/58						+8			
22.5/54				+7					
25.0/100	+2								
30.0/100	+2								
35.0/100	+3								
41.5/100	+4			+7	+5	+8			
45.0/100	+4								

Examination of the feedback obtained for run 28B at 22.5 MWt with full and reduced flow seems to indicate that an adjustment is also necessary for these experiments. The feedback obtained without adjustment of rod worth is shown in Figs. 29 and 30.

Average rod worth and feedback magnitude at 2 sec after the rod drops at 41.5 MWt were computed for comparable experiments performed during runs 25, 26B, and 28A through 29A. The averages were \$0.0441 for rod worth and \$0.0096 for feedback. The standard deviations were \$0.0045 for rod worth and \$0.0021 for feedback.

Note that rod-drop data taken during and after run 28A were sampled at the standard sampling rate during the first 2 sec (200 samples/sec), but the sampling rate was reduced by a factor of two after 2 sec. This allowed recording of data for longer times following the rod drop without sacrificing definition of power during the period of rapid change immediately after the rod drop. Note also that the initial power is averaged for 24 samples taken at the initial sampling rate to obtain an average to which the data can be normalized.

Data obtained more than 30 sec after a rod drop may be unreliable, as the bulk-sodium temperature does not necessarily remain constant for longer times.

C. Feedback Modeling

Feedback models were developed from both oscillator and rod-drop data taken during run 26.[2]

Development of a time-domain model for the feedback which closely approximates the feedback as measured by the methods of Ref. 2 requires from five to seven terms in Eq. 3 if the approximation is to be good over a time span of about 30 sec following the rod drop.

Models developed from rod-drop data obtained during runs 29A and 29C are shown in Figs. 52 and 53.

Feedback in both the oscillator and rod-drop experiments is the "negative" feedback of the reactor system, in the sense that negative feedback inhibits change.

IV. SUMMARY

Rod-drop experiments have provided the greatest contribution to this report; however, it is desirable to compare results obtained by this method to results obtained from oscillator experiments. The tables and plots in this report provide much data for this comparison and for other studies involving the performance of EBR-II.

When results from the reactor runs covered here are compared, the reactor loading and the inner-blanket material must be considered. Gross differences may be implied by a significant change in the grid loading. Table I indicates the changes in grid loading, and Ref. 5 gives diagrams for the loadings covered in this report.

APPENDIX A

Tabulated Oscillator Data

TABLE IV. Computed Open-loop Transfer Function, $G_0(s)$

Frequency of Oscillation, Hz	Amplitude, $\frac{\Delta n/n}{\Delta k/k}$	Phase, deg	Frequency of Oscillation, Hz	Amplitude, $\frac{\Delta n/n}{\Delta k/k}$	Phase, deg
0.00100	1837.8000	-77.9720	0.35000	143.2300	-8.9852
0.00150	1279.6000	-73.1350	0.40000	141.8500	-8.2009
0.00200	1006.7000	-69.0810	0.45000	140.7800	-7.5450
0.00250	845.6600	-65.6430	0.50000	139.9300	-6.9875
0.00300	739.6800	-62.6850	0.60000	138.6600	-6.0890
0.00350	664.8800	-60.1150	0.70000	137.7700	-5.3942
0.00400	609.3900	-57.8710	0.80000	137.1300	-4.8396
0.00450	566.6200	-55.9070	0.90000	136.6500	-4.3862
0.00500	532.6200	-54.1840	1.00000	136.2800	-4.0085
0.00600	481.7700	-51.3380	1.50000	135.2900	-2.7909
0.00700	445.1400	-49.1160	2.00000	134.8900	-2.1352
0.00800	417.0600	-47.3480	2.50000	134.7000	-1.7291
0.00900	394.5000	-45.9100	3.00000	134.5900	-1.4545
0.01000	375.7600	-44.7110	3.50000	134.5200	-1.2573
0.01500	313.2700	-40.5850	4.00000	134.4800	-1.1092
0.02000	276.5100	-37.7810	4.50000	134.4500	-0.9943
0.02500	251.9000	-35.5120	5.00000	134.4300	-0.9028
0.03000	234.1800	-33.5460	6.00000	134.4000	-0.7670
0.03500	220.8300	-31.7880	7.00000	134.3800	-0.6719
0.04000	210.4600	-30.1900	8.00000	134.3700	-0.6023
0.04500	202.2200	-28.7290	9.00000	134.3700	-0.5497
0.05000	195.5600	-27.3910	10.00000	134.3600	-0.5091
0.06000	185.5600	-25.0470	20.00000	134.3400	-0.3676
0.07000	178.4900	-23.0870	30.00000	134.3400	-0.3704
0.08000	173.2700	-21.4470	40.00000	134.3400	-0.4095
0.09000	169.2600	-20.0670	50.00000	134.3300	-0.4630
0.10000	166.0800	-18.8970	60.00000	134.3300	-0.5237
0.15000	156.3500	-14.9990	70.00000	134.3300	-0.5886
0.20000	151.0100	-12.7230	80.00000	134.3300	-0.6561
0.25000	147.5100	-11.1430	90.00000	134.3300	-0.7253
0.30000	145.0400	-9.9422	100.00000	134.3200	-0.7957

TABLE V. Computed and Measured Open-loop Transfer Function, $G_0(s)$

Frequency of Oscillation, Hz	Amplitude, comp	Phase, comp	Amplitude, meas	Phase, meas
8.80300	1.34370E+02	-5.54000E-01	1.34370E+02	-5.54000E-01
6.15600	1.34401E+02	-7.45000E-01	1.34509E+02	-6.88000E-01
4.00900	1.34481E+02	-1.10000E-00	1.34233E+02	-1.02600E-00
1.97300	1.34895E+02	-2.15100E-00	1.35070E+02	-2.21900E-00
0.97400	1.36329E+02	-4.09100E-00	1.36158E+02	-3.86000E-00
0.79800	1.37097E+02	-4.84000E-00	1.37194E+02	-4.76800E-00
0.60300	1.38580E+02	-6.06500E-00	1.38629E+-2	-6.09000E-00
0.49900	1.39893E+02	-7.00000E-00	1.40102E+02	-7.05000E-00
0.40000	1.41805E+02	-8.02050E-00	1.41934E+02	-8.08200E-00
0.30100	1.44948E+02	-9.92300E-00	1.44950E+02	-9.80200E-00
0.20000	1.50968E+02	-1.27260E+01	1.51069E+02	-1.27170E+01
0.09900	1.66226E+02	-1.89630E+01	1.66521E+02	-1.90040E+01

TABLE VI. Run 26B Transfer Function at 22.5 MWt, $G_0(s)$ and $G(s)$

Frequency of Oscillation, Hz	Open-loop Amplitude, $\frac{\Delta n/n}{\Delta k/k}$	Open-loop Phase, deg	Closed-loop Amplitude, $\frac{\Delta n/n}{\Delta k/k}$	Closed-loop Phase, deg
6.21072	1.34401E+02	-7.43957E-01	1.34338E+02	-2.52498E-01
4.05057	1.34482E+02	-1.09595E-00	1.34241E+02	-4.64583E-01
2.50105	1.34703E+02	-1.72812E-00	1.34403E+02	-4.49441E-01
1.50223	1.35289E+02	-2.78674E-00	1.34808E+02	-1.25909E-00
1.15661	1.35853E+02	-3.52912E-00	1.34025E+02	-1.57920E-00
0.96477	1.36401E+02	-4.13384E-00	1.34560E+02	-1.85357E-00
0.79985	1.37136E+02	-4.83999E-00	1.34043E+02	-2.39816E-00
0.58380	1.38837E+02	-6.21813E-00	1.33116E+02	-3.44777E-00
0.50102	1.39915E+02	-6.97667E-00	1.33110E+02	-4.51868E-00
0.39948	1.41869E+02	-8.20790E-00	1.33634E+02	-5.79899E-00
0.30027	1.45033E+02	-9.93589E-00	1.35071E+02	-7.97105E-00
0.20023	1.50994E+02	-1.27150E+01	1.39924E+02	-1.17877E+01
0.20027	1.50990E+02	-1.27133E+01	1.38974E+02	-1.13321E+01
0.19980	1.51029E+02	-1.27306E+01	1.38941E+02	-1.04134E+01
0.13980	1.57822E+02	-1.56108E+01	1.44604E+02	-1.48458E+01
0.09955	1.66213E+02	-1.89458E+01	1.53841E+02	-1.92900E+01
0.09953	1.66216E+02	-1.89470E+01	1.52087E+02	-1.88693E+01
0.08016	1.73200E+02	-2.14226E+01	1.58301E+02	-2.20575E+01
0.08014	1.73209E+02	-2.14252E+01	1.56158E+02	-2.21753E+01
0.08013	1.73212E+02	-2.14266E+01	1.58898E+02	-2.20212E+01
0.06063	1.85039E+02	-2.49115E+01	1.67990E+02	-2.61025E+01
0.06064	1.85034E+02	-2.49101E+01	1.71378E+02	-2.55255E+01
0.04070	2.09182E+02	-2.99755E+01	1.91389E+02	-3.07485E+01
0.04071	2.09174E+02	-2.99741E+01	1.91909E+02	-3.10898E+01
0.01985	2.77374E+02	-3.78529E+01	2.55994E+02	-4.04656E+01
0.01985	2.77401E+02	-3.78552E+01	2.55298E+02	-3.98952E+01
0.00987	3.77936E+02	-4.48496E+01	3.49441E+02	-4.49636E+01
0.00987	3.77926E+02	-4.48490E+01	3.51002E+02	-4.67775E+01
0.00782	4.21600E+02	-4.76364E+01	3.98403E+02	-5.00926E+01
0.00567	4.96201E+02	-5.21772E+01	4.66393E+02	-5.33643E+01

TABLE VII. Run 26B Feedback at 22.5 MWt, H(s)

Frequency of Oscillation, Hz	Amplitude, $\frac{\Delta k/k}{\Delta n/n}$	Phase, deg	Real Part	Imaginary Part
6.21072	6.39332E-05	-8.63349E+01	4.08690E-06	-6.38025E-05
4.05057	8.30959E-05	-7.99647E+01	1.44798E-05	-8.18244E-05
2.50105	1.66687E-04	-8.31938E+01	1.97543E-05	-1.65512E-04
1.50223	1.99175E-04	-8.03740E+01	3.33054E-05	-1.96371E-04
1.15661	2.71445E-04	-6.57432E+01	1.11517E-04	-2.47480E-04
0.96477	3.10395E-04	-6.81565E+01	1.15489E-04	-2.88110E-04
0.79985	3.56504E-04	-5.82301E+01	1.87703E-04	-3.03089E-04
0.58380	4.71501E-04	-4.41425E+01	3.38354E-04	-3.28374E-04
0.50102	4.81991E-04	-3.49721E+01	3.94959E-04	-2.76266E-04
0.39948	5.30964E-04	-2.81177E+01	4.68300E-04	-2.50235E-04
0.30027	5.64431E-04	-1.67902E+01	5.40369E-04	-1.63046E-04
0.20023	5.35669E-04	2.44962E-01	5.35664E-04	2.29018E-06
0.20027	5.96321E-04	-4.19686E-00	5.94722E-04	-4.36409E-05
0.19980	6.40145E-04	-1.43079E+01	6.20289E-04	-1.58200E-04
0.13980	5.85901E-04	6.54325E-00	5.82084E-04	6.67653E-05
0.09955	4.85295E-04	2.35598E+01	4.44842E-04	1.93975E-04
0.09953	5.58992E-04	1.80320E+01	5.31537E-04	1.73034E-04
0.08016	5.47537E-04	2.87673E+01	4.79961E-04	2.63504E-04
0.08014	6.35379E-04	2.90062E+01	5.55682E-04	3.08098E-04
0.08013	5.23849E-04	2.85881E+01	4.59982E-04	2.50666E-04
0.06063	5.61007E-04	3.76516E+01	4.44171E-04	3.42696E-04
0.06064	4.34825E-04	3.31960E+01	3.63863E-04	2.38069E-04
0.04070	4.49525E-04	3.89966E+01	3.49363E-04	2.82874E-04
0.04071	4.40935E-04	4.32765E+01	3.21024E-04	3.02270E-04
0.01985	3.46318E-04	6.87934E+01	1.25274E-04	3.22866E-04
0.01985	3.39566E-04	6.20988E+01	1.58899E-04	3.00093E-04
0.00987	2.15827E-04	4.63606E+01	1.48946E-04	1.56193E-04
0.00987	2.23015E-04	7.03096E+01	7.51421E-05	2.09975E-04
0.00782	1.73234E-04	8.60194E+01	1.20257E-05	1.72816E-04
0.00567	1.35811E-04	7.12677E+01	4.36155E-05	1.28617E-04

TABLE VIII. Run 26B Transfer Function at 30 MWt, $G_o(s)$ and G(s)

Frequency of Oscillation, Hz	Open-loop Amplitude, $\frac{\Delta n/n}{\Delta k/k}$	Open-loop Phase, deg	Closed-loop Amplitude, $\frac{\Delta n/n}{\Delta k/k}$	Closed-loop Phase, deg
4.02251	1.34484E+02	-1.10309E-00	1.34275E+02	-9.64883E-02
1.99498	1.34899E+02	-2.13992E-00	1.34126E+02	-4.68658E-01
0.89671	1.36666E+02	-4.39944E-00	1.32630E+02	-1.04103E-00
0.59219	1.38746E+02	-6.15035E-00	1.31881E+02	-2.24451E-00
0.40652	1.41702E+02	-8.10849E-00	1.31116E+02	-4.56194E-00
0.20175	1.50866E+02	-1.26590E+01	1.35368E+02	-1.03226E+01
0.09757	1.66795E+02	-1.91640E+01	1.48925E+02	-1.81991E+01

TABLE IX. Run 26B Feedback at 30 MWt, H(s)

Frequency of Oscillation, Hz	Amplitude, $\frac{\Delta k/k}{\Delta n/n}$	Phase, deg	Real Part	Imaginary Part
4.02251	1.31244E-04	-8.43509E+01	1.29191E-05	-1.30607E-04
1.99498	2.21017E-04	-7.75427E+01	4.76761E-05	-2.15813E-04
0.89671	4.88953E-04	-6.02013E+01	2.42987E-04	-4.24302E-04
0.59219	6.28172E-04	-4.91587E+01	4.10803E-04	-4.75227E-04
0.40652	7.28565E-04	-3.22496E+01	6.16171E-04	-3.88768E-04
0.20175	8.10699E-04	-9.14675E-00	8.00394E-04	-1.28872E-04
0.09757	7.27260E-04	1.02198E+01	7.15722E-04	1.29033E-04

TABLE X. Run 26B Transfer Function at 41.5 MWt, $G_0(s)$ and G(s)

Frequency of Oscillation, Hz	Open-loop Amplitude, $\frac{\Delta n/n}{\Delta k/k}$	Open-loop Phase, deg	Closed-loop Amplitude, $\frac{\Delta n/n}{\Delta k/k}$	Closed-loop Phase, deg
4.07902	1.34480E+02	-1.08883E-00	1.34189E+02	2.84245E-01
1.98246	1.34906E+02	-2.15263E-00	1.34105E+02	-8.64840E-02
1.49922	1.35292E+02	-2.79188E-00	1.34180E+02	-2.86904E-01
0.99243	1.36306E+02	-4.03458E-00	1.33187E+02	-4.82834E-01
0.79887	1.37141E+02	-4.84487E-00	1.33032E+02	-1.04630E-00
0.59829	1.38681E+02	-6.10200E-00	1.31911E+02	-1.77460E-00
0.47889	1.40269E+02	-7.21199E-00	1.31750E+02	-2.80068E-00
0.39631	1.41946E+02	-8.25351E-00	1.30393E+02	-3.64862E-00
0.30175	1.44971E+02	-9.90460E-00	1.32121E+02	-5.95521E-00
0.19963	1.51044E+02	-1.27371E+01	1.34634E+02	-1.00428E+01

TABLE XI. Run 26B Feedback at 41.5 MWt, H(s)

Frequency of Oscillation, Hz	Amplitude, $\frac{\Delta k/k}{\Delta n/n}$	Phase, deg	Real Part	Imaginary Part
4.07902	1.79118E-04	-8.44288E+01	1.73892E-05	-1.78272E-04
1.98246	2.71718E-04	-7.95041E+01	4.94976E-05	-2.67171E-04
1.49922	3.30195E-04	-7.77714E+01	6.99396E-05	-3.22703E-04
0.99243	4.91033E-04	-6.72729E+01	1.89706E-04	-4.52907E-04
0.79887	5.39970E-04	-6.24138E+01	2.50050E-04	-4.78584E-04
0.59829	6.69788E-04	-5.25505E+01	4.07273E-04	-5.31738E-04
0.47889	7.30115E-04	-4.58802E+01	5.08277E-04	-5.24139E-04
0.39631	8.59315E-04	-3.75132E+01	6.81620E-04	-5.23275E-04
0.30175	8.35505E-04	-2.86998E+01	7.32868E-04	-4.01229E-04
0.19963	8.71718E-04	-1.08745E+01	8.56063E-04	-1.64456E-04

TABLE XII. Run 26C Transfer Function at 22.5 MWt, $G_o(s)$ and G(s)

Frequency of Oscillation, Hz	Open-loop Amplitude, $\frac{\Delta n/n}{\Delta k/k}$	Open-loop Phase, deg	Closed-loop Amplitude, $\frac{\Delta n/n}{\Delta k/k}$	Closed-loop Phase, deg
5.97874	1.34406E+02	-7.69127E-01	1.34337E+02	-2.58736E-01
4.04312	1.34483E+02	-1.09784E-00	1.34360E+02	-6.24392E-01
1.99667	1.34898E+02	-2.13822E-00	1.34586E+02	-1.05572E-00
1.50468	1.35286E+02	-2.78257E-00	1.34510E+02	-1.25212E-00
0.98317	1.36337E+02	-4.06728E-00	1.34663E+02	-2.05487E-00
0.97244	1.36374E+02	-4.10583E-00	1.34139E+02	-1.68191E-00
0.95359	1.36442E+02	-4.17532E-00	1.33824E+02	-2.31793E-00
0.89042	1.36693E+02	-4.42567E-00	1.34225E+02	-2.68513E-00
0.75369	1.37409E+02	-5.08155E-00	1.34884E+02	-3.28112E-00
0.60220	1.38640E+02	-6.07134E-00	1.34260E+02	-3.89580E-00
0.40013	1.41854E+02	-8.19862E-00	1.34173E+02	-6.13545E-00
0.29830	1.45115E+02	-9.97794E-00	1.35585E+02	-8.35971E-00
0.19663	1.51301E+02	-1.28493E+01	1.40361E+02	-1.21690E+01
0.19960	1.51047E+02	-1.27382E+01	1.39912E+02	-1.16751E+01
0.09858	1.66494E+02	-1.90513E+01	1.52814E+02	-1.92889E+01
0.09840	1.66548E+02	-1.90717E+01	1.53689E+02	-1.96681E+01
0.79063	1.73440E+02	-2.15017E+01	1.59986E+02	-2.24161E+01
0.05751	1.87717E+02	-2.55911E+01	1.73655E+02	-2.68831E+01
0.02775	2.41495E+02	-3.44002E+01	2.22230E+02	-3.62588E+01
0.02773	2.21561E+02	-3.44077E+01	2.23766E+02	-3.66278E+01
0.01386	3.24418E+02	-4.13540E+01	3.07029E+02	-4.32806E+01
0.00881	3.98344E+02	-4.61557E+01	3.74581E+02	-4.86341E+01

TABLE XIII. Run 26C Feedback at 22.5 MWt, H(s)

Frequency of Oscillation, Hz	Amplitude, $\frac{\Delta k/k}{\Delta n/n}$	Phase, deg	Real Part	Imaginary Part
5.97874	6.64032E-05	-8.61921E+01	4.40989E-06	-6.62566E-05
4.04312	6.18461E-05	-8.28405E+01	7.70796E-06	-6.13639E-05
1.99667	1.41265E-04	-8.14086E+01	2.11031E-05	-1.39680E-04
1.50468	2.02537E-04	-7.58399E+01	4.95472E-05	-1.96383E-04
0.98317	2.74774E-04	-6.75591E+01	1.04889E-04	-2.53967E-04
0.97244	3.35780E-04	-6.57741E+01	1.37781E-04	-3.06209E-04
0.95359	2.79470E-04	-5.58936E+01	1.56707E-04	-2.31400E-04
0.89042	2.61769E-04	-5.55092E+01	1.48232E-04	-2.15754E-04
0.75369	2.67997E-04	-5.52767E+01	1.52654E-04	-2.20270E-04
0.60220	3.64456E-04	-4.48075E+01	2.58573E-04	-2.56842E-04
0.40013	4.80603E-04	-2.57400E+01	4.32915E-04	-2.08720E-04
0.29830	5.24539E-04	-1.34173E+01	5.10222E-04	-1.21715E-04
0.19663	5.21573E-04	+3.51412E-00	5.20592E-04	+3.19696E-05
0.19960	5.42128E-04	-1.42114E-00	5.41962E-04	-1.34453E-05
0.09858	5.38296E-04	+2.19408E+01	4.99307E-04	+2.01133E-04
0.09840	5.06550E-04	+2.67558E+01	4.52315E-04	+2.28042E-04
0.07963	4.94221E-04	+3.31460E+01	4.13801E-04	+2.70227E-04
0.05751	4.49074E-04	+4.23967E+01	3.31638E-04	+3.02792E-04
0.02775	3.85303E-04	+5.66577E+01	2.11777E-04	+3.21883E-04
0.02773	3.69000E-04	+6.23870E+01	1.71029E-04	+3.26970E-04
0.01386	2.04521E-04	+7.37238E+01	5.73211E-05	+1.96324E-04
0.00881	1.94679E-04	+8.25253E+01	2.53255E-05	+1.93025E-04

TABLE XIV. Run 26C Transfer Function at 30 MWt, $G_0(s)$ and G(s)

Frequency of Oscillation, Hz	Open-loop Amplitude, $\frac{\Delta n/n}{\Delta k/k}$	Open-loop Phase, deg	Closed-loop Amplitude, $\frac{\Delta n/n}{\Delta k/k}$	Closed-loop Phase, deg
6.00333	1.34406E+02	-7.66359E-01	1.34312E+02	-8.87278E-02
4.01382	1.34485E+02	-1.10532E-00	1.34433E+02	-2.00839E-01
2.46812	1.34713E+02	-1.74998E-00	1.34659E+02	-6.13599E-01
1.48319	1.35311E+02	-2.81957E-00	1.34140E+02	-8.64853E-01
0.99844	1.36286E+02	-4.01360E-00	1.33946E+02	-1.34883E-00
0.99988	1.36281E+02	-4.00861E-00	1.34197E+02	-1.25802E-00
0.87928	1.36742E+02	-4.47287E-00	1.33832E+02	-1.54334E-00
0.79234	1.37178E+02	-4.87777E-00	1.33294E+02	-1.76971E-00
0.69482	1.37817E+02	-5.42592E-00	1.32781E+02	-2.06388E-00
0.60073	1.38655E+02	-6.08286E-00	1.32713E+02	-2.58934E-00
0.44364	1.40908E+02	-7.62205E-00	1.30960E+02	-4.17283E-00
0.35200	1.43169E+02	-8.95034E-00	1.32101E+02	-5.83380E-00
0.20224	1.50825E+02	-1.26411E+01	1.34614E+02	-1.06136E+01
0.13908	1.57933E+02	-1.56565E+01	1.42998E+02	-1.42203E+01
0.09793	1.66688E+02	-1.91240E+01	1.51471E+02	-1.77199E+01

TABLE XV. Run 26C Feedback at 30 MWt, H(s)

Frequency of Oscillation, Hz	Amplitude, $\frac{\Delta k/k}{\Delta n/n}$	Phase, deg	Real Part	Imaginary Part
6.00333	8.81763E-05	-8.62079E+01	5.83159E-06	-8.79828E-05
4.01382	1.17458E-04	-8.76630E+01	4.78959E-06	-1.17366E-04
2.46812	1.47284E-04	-8.76748E+01	5.97549E-06	-1.47163E-04
1.48319	2.61298E-04	-7.38725E+01	7.25824E-05	-2.51015E-04
0.99844	3.67290E-04	-6.68979E+01	1.44113E-04	-3.37836E-04
0.99988	3.72797E-04	-6.95721E+01	1.30116E-04	-3.49352E-04
0.87928	4.09999E-04	-6.41826E+01	1.78555E-04	-3.69076E-04
0.79234	4.53865E-04	-5.87874E+01	2.35198E-04	-3.88168E-04
0.69482	5.13643E-04	-5.38752E+01	3.02815E-04	-4.14887E-04
0.60073	5.53409E-04	-4.99838E+01	3.55843E-04	-4.23835E-04
0.44364	6.97793E-04	-3.35538E+01	5.81517E-04	-3.85684E-04
0.35200	7.06310E-04	-2.66891E+01	6.31057E-04	-3.17238E-04
0.20224	8.36175E-04	-5.67808E-00	8.32075E-04	-8.27306E-05
0.13908	6.81980E-04	+7.63514E-01	6.81919E-04	+9.08764E-06
0.09793	6.22108E-04	+4.05149E-00	6.20553E-04	+4.39538E-04

TABLE XVI. Run 26C Transfer Function at 41.5 MWt, $G_o(s)$ and G(s)

Frequency of Oscillation, Hz	Open-loop Amplitude, $\frac{\Delta n/n}{\Delta k/k}$	Open-loop Phase, deg	Closed-loop Amplitude, $\frac{\Delta n/n}{\Delta k/k}$	Closed-loop Phase, deg
4.04085	1.34483E+02	-1.09841E-00	1.34186E+02	+2.87392E-02
2.15827	1.34822E+02	-1.98694E-00	1.34065E+02	+2.56881E-02
1.49933	1.35292E+02	-2.79169E-00	1.33436E+02	-2.40217E-01
0.95816	1.36425E+02	-4.15828E-00	1.32649E+02	-3.19455E-01
0.82701	1.36991E+02	-4.70805E-00	1.32107E+02	-9.61468E-01
0.71237	1.37688E+02	-5.31856E-00	1.31784E+02	-1.28777E-00
0.52761	1.39530E+02	-6.71357E-00	1.30583E+02	-2.75963E-00
0.39678	1.41935E+02	-8.24675E-00	1.30442E+02	-3.96690E-00
0.30150	1.44981E+02	-9.90987E-00	1.30827E+02	-6.37130E-00

TABLE XVII. Run 26C Feedback at 41.5 MWt, H(s)

Frequency of Oscillation, Hz	Amplitude, $\frac{\Delta k/k}{\Delta n/n}$	Phase, deg	Real Part	Imaginary Part
4.04085	1.80794E-04	-8.43764E+01	1.77163E-05	-1.79923E-04
2.15827	2.64598E-04	-7.99150E+01	4.63337E-05	-2.60509E-04
1.49933	3.46988E-04	-7.12519E+01	1.11523E-04	-3.28577E-04
0.95816	5.39897E-04	-6.50422E+01	2.27809E-04	-4.89480E-04
0.82701	5.55902E-04	-5.81366E+01	2.93458E-04	-4.72132E-04
0.71237	6.15208E-04	-5.47938E+01	3.54678E-04	-5.02675E-04
0.52761	7.08779E-04	-4.14468E+01	5.31279E-04	-4.69157E-04
0.36978	8.28578E-04	-3.54210E+01	6.75225E-04	-4.80231E-04
0.30150	8.70572E-04	-2.29035E+01	8.01941E-04	-3.38811E-04

APPENDIX B

Plotted Oscillator Results

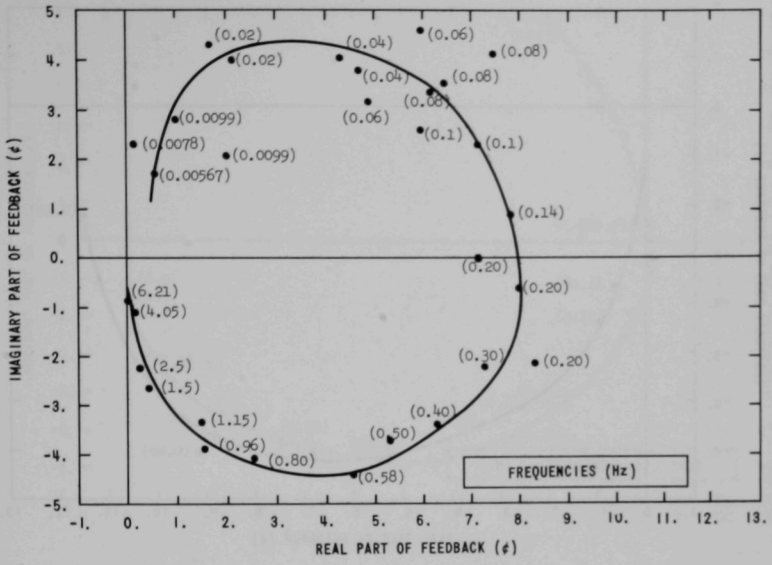

Fig. 5. Nyquist Plot of Run 26B Feedback at 22.5 MWt

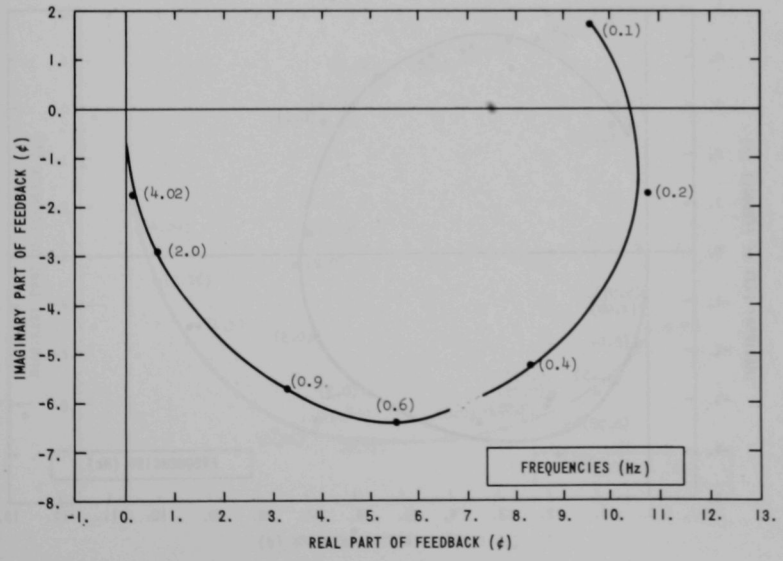

Fig. 6. Nyquist Plot of Run 26B Feedback at 30 MWt

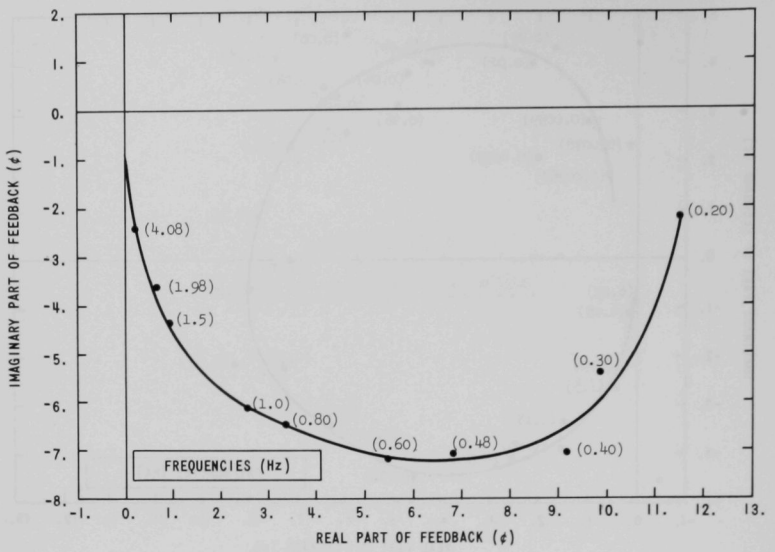

Fig. 7. Nyquist Plot of Run 26B Feedback at 41.5 MWt

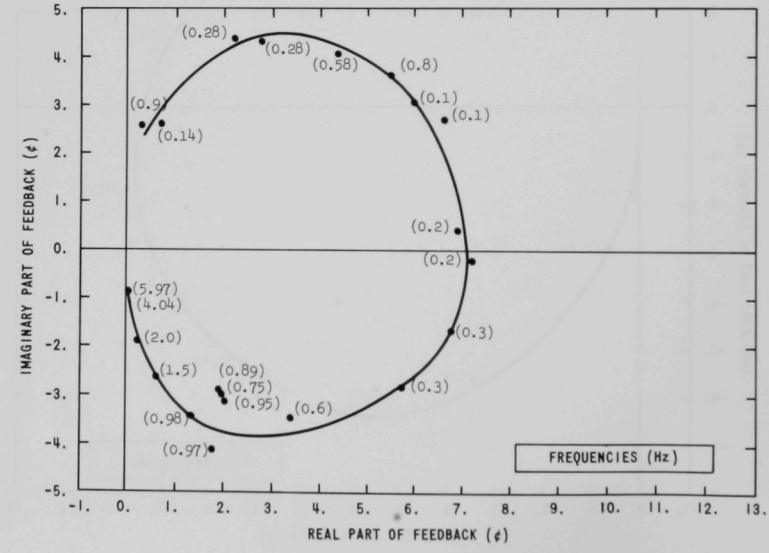

Fig. 8. Nyquist Plot of Run 26C Feedback at 22.5 MWt

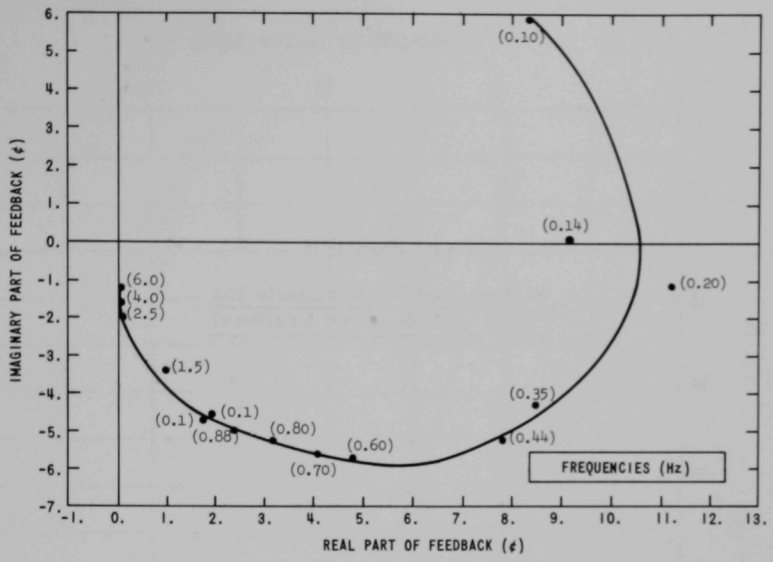

Fig. 9. Nyquist Plot of Run 26C Feedback at 30 MWt

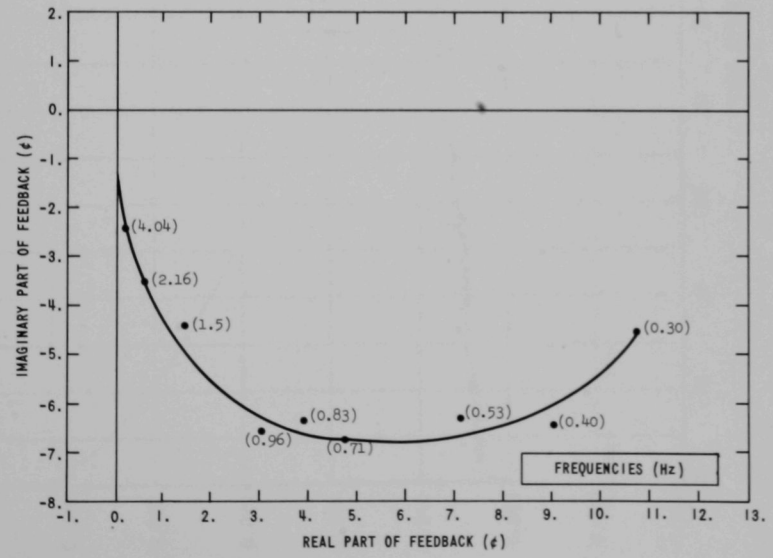

Fig. 10. Nyquist Plot of Run 36C Feedback at 41.5 MWt

APPENDIX C

Plotted Rod-drop Results for Power and Negative Feedback

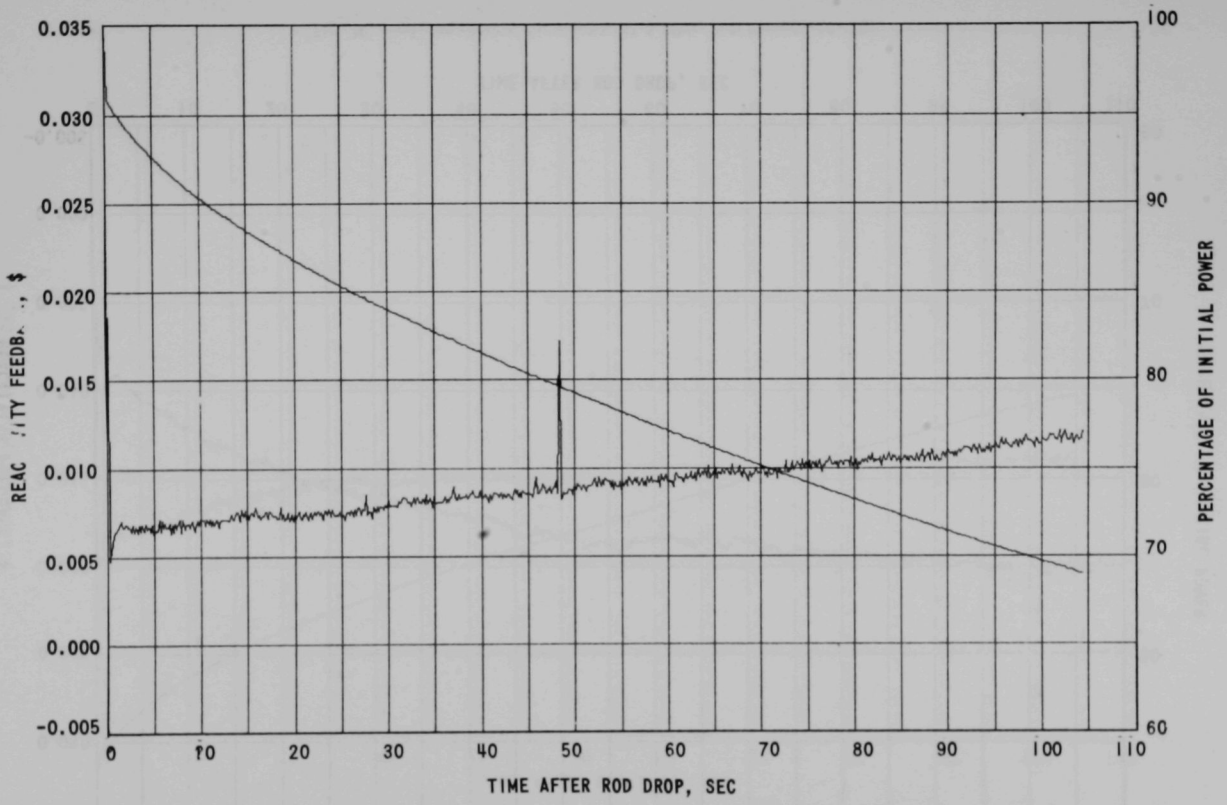

Fig. 11. Rod-drop Results for Run 25, 22.5 MWt, Full Flow (5-15-67)

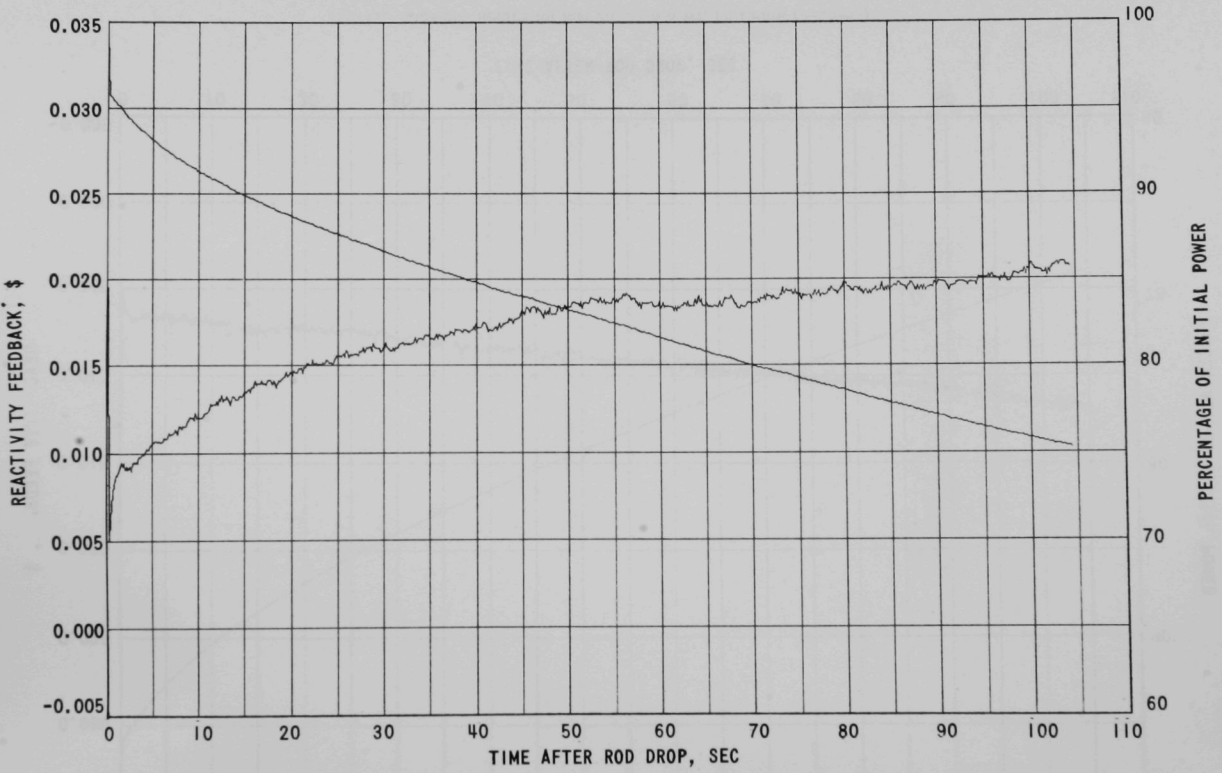

Fig. 12. Rod-drop Results for Run 25, 41.5 MWt, Full Flow (5-16-67)

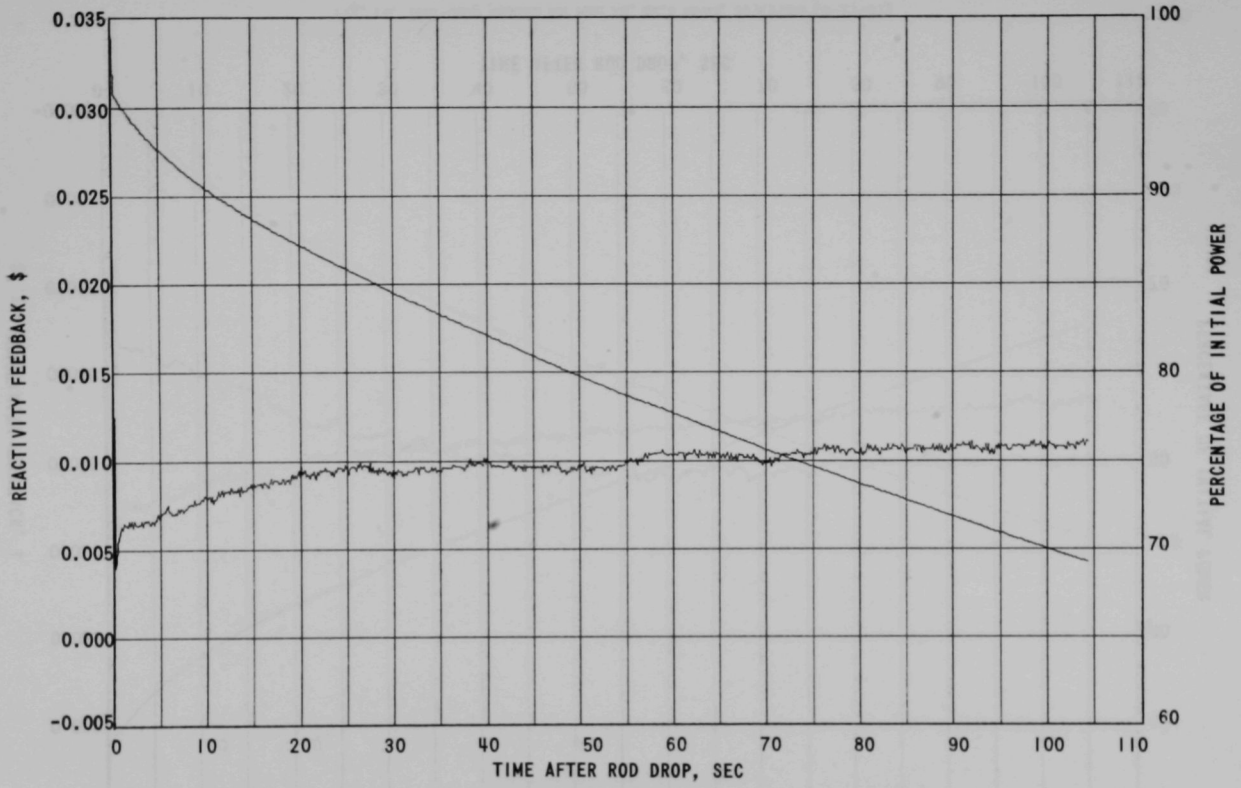

Fig. 13. Rod-drop Results for Run 25, 22.5 MWt, 75% Flow (5-17-67)

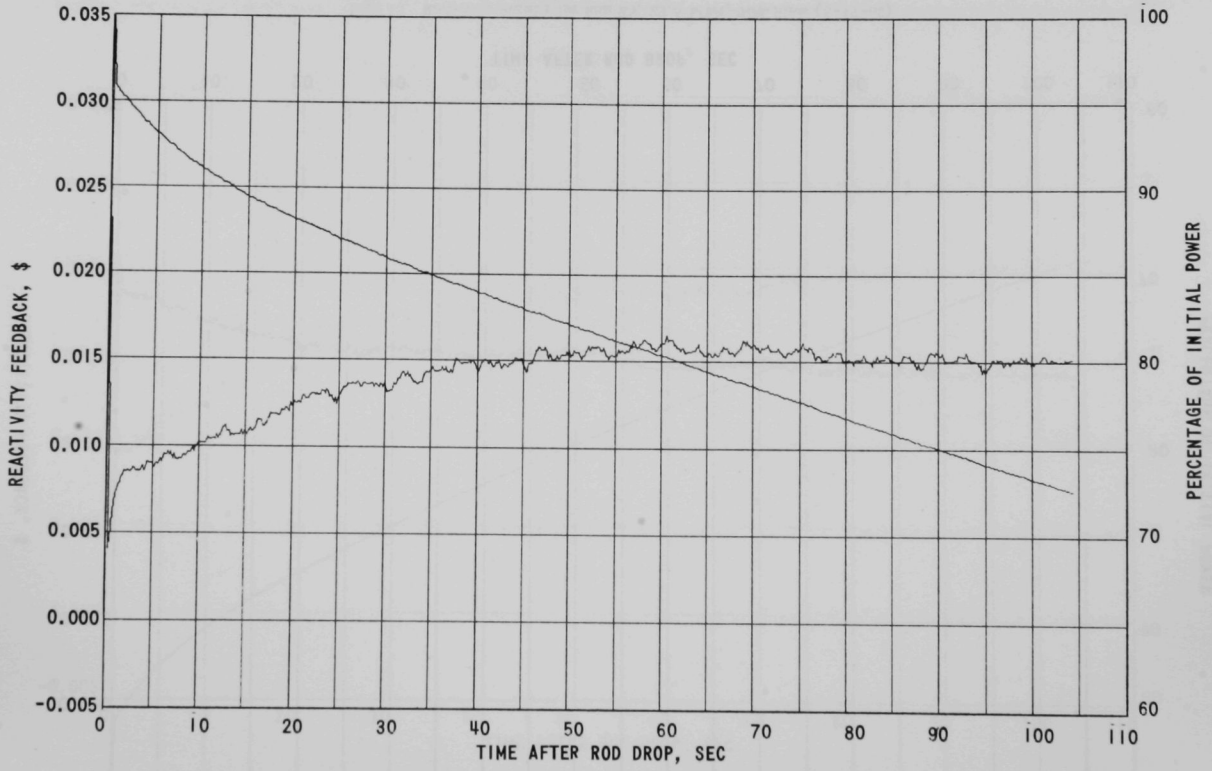

Fig. 14. Rod-drop Results for Run 25, 22.5 MWt, 50% Flow (5-17-67)

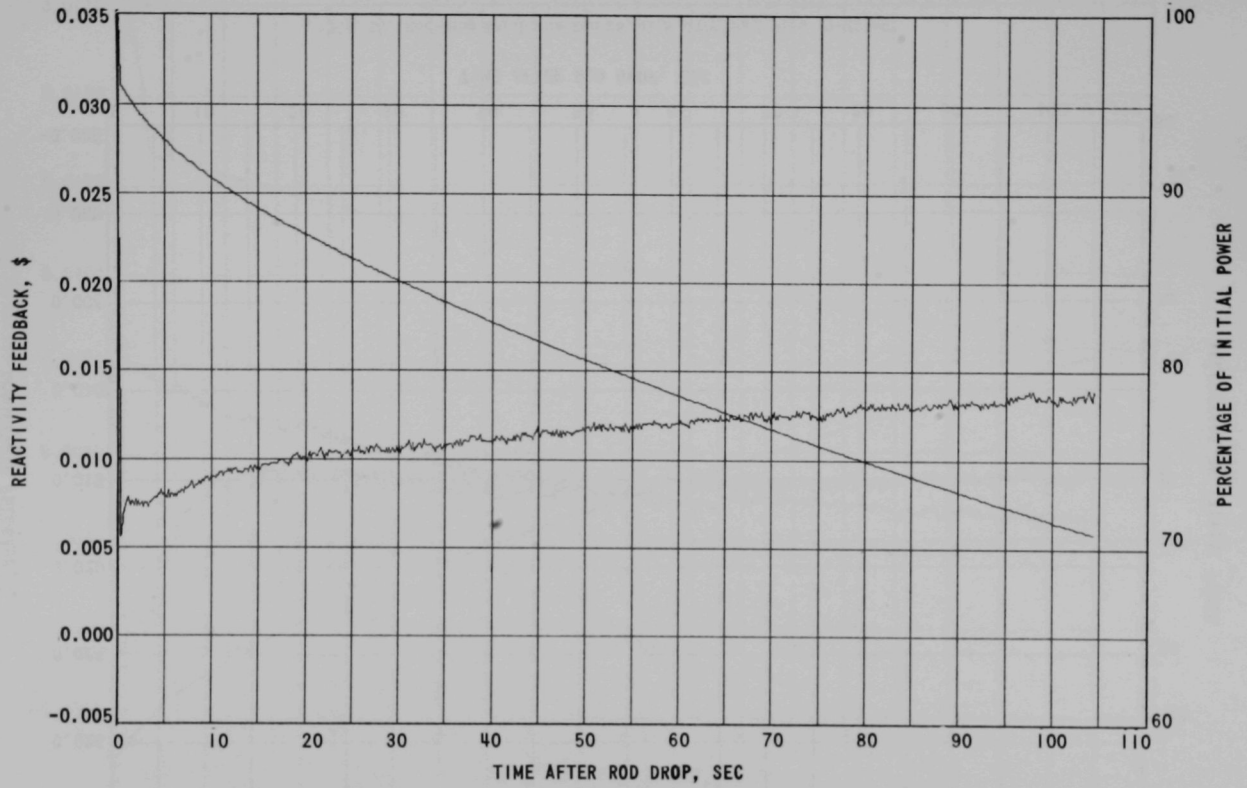

Fig. 15. Rod-drop Results for Run 25, 30 MWt, 100% Flow (5-17-67)

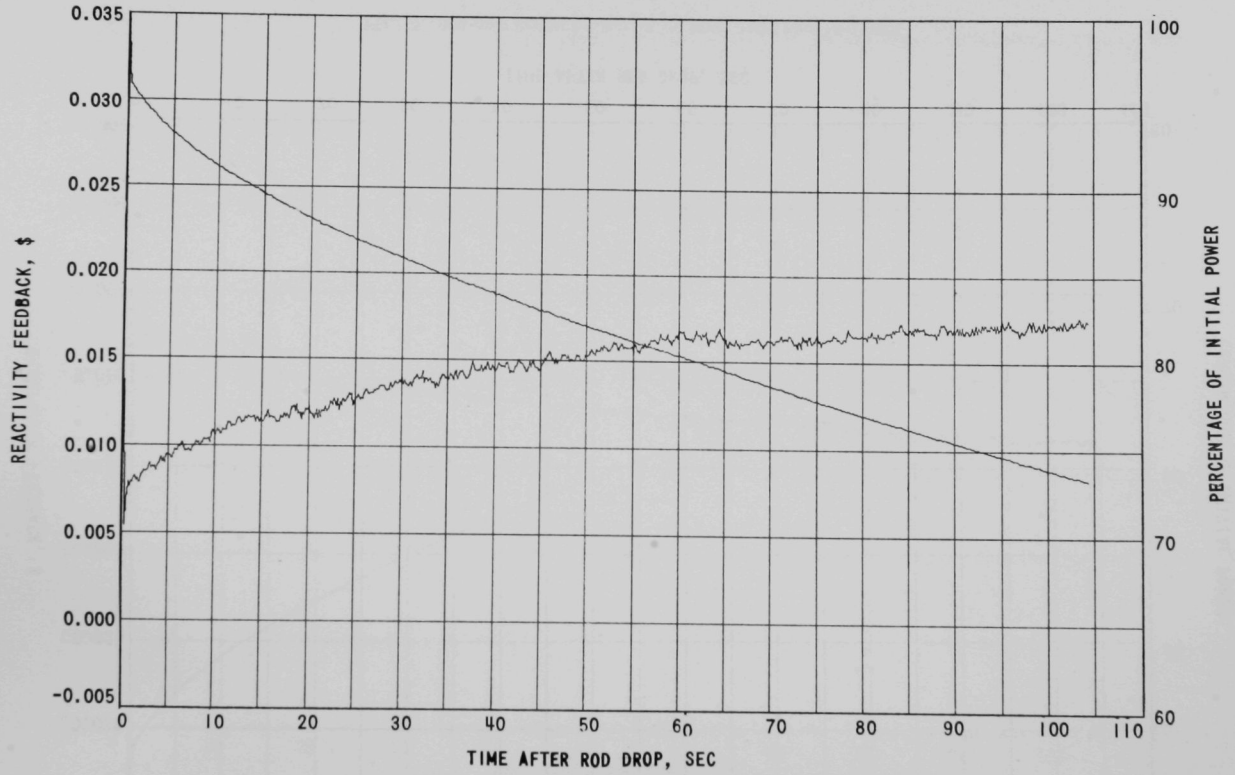

Fig. 16. Rod-drop Results for Run 25, 41.5 MWt, Full Flow (7-23-67)

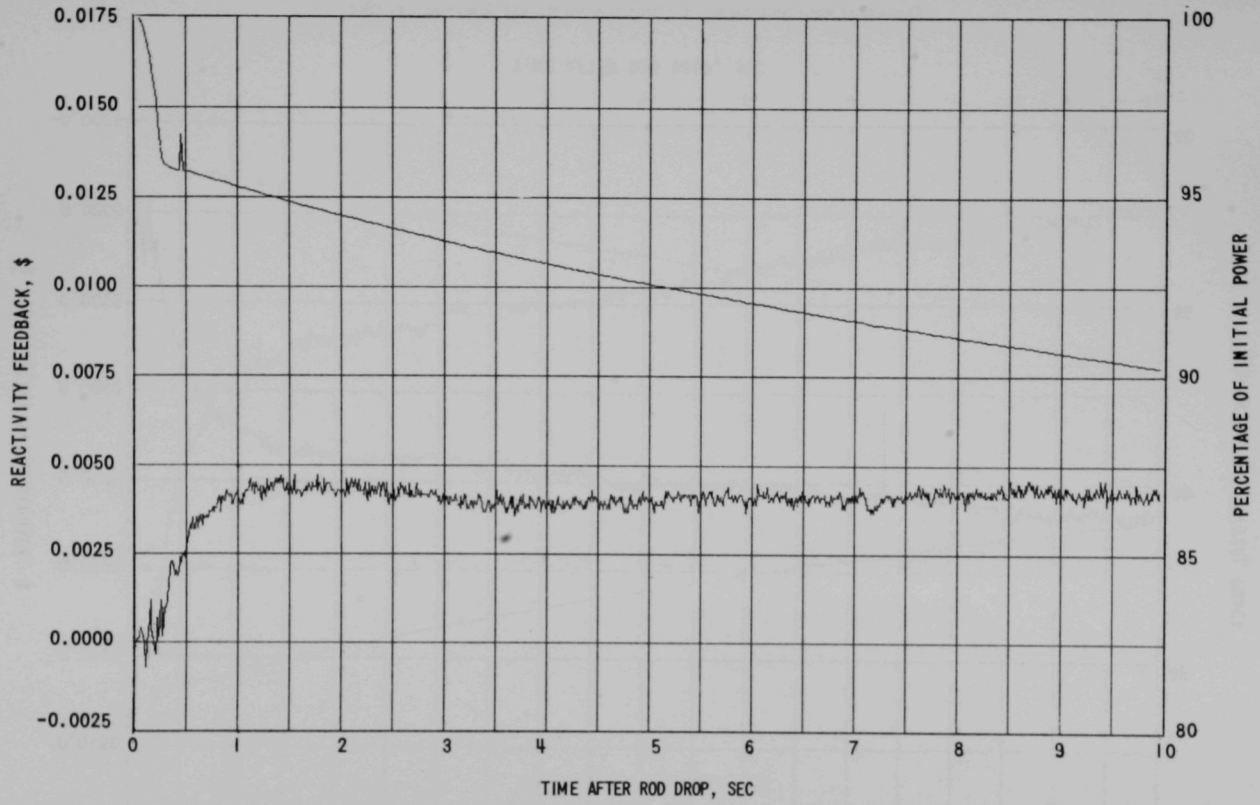

Fig. 17. Rod-drop Results for Run 26A, 25.0 MWt, Full Flow (9-26-67)

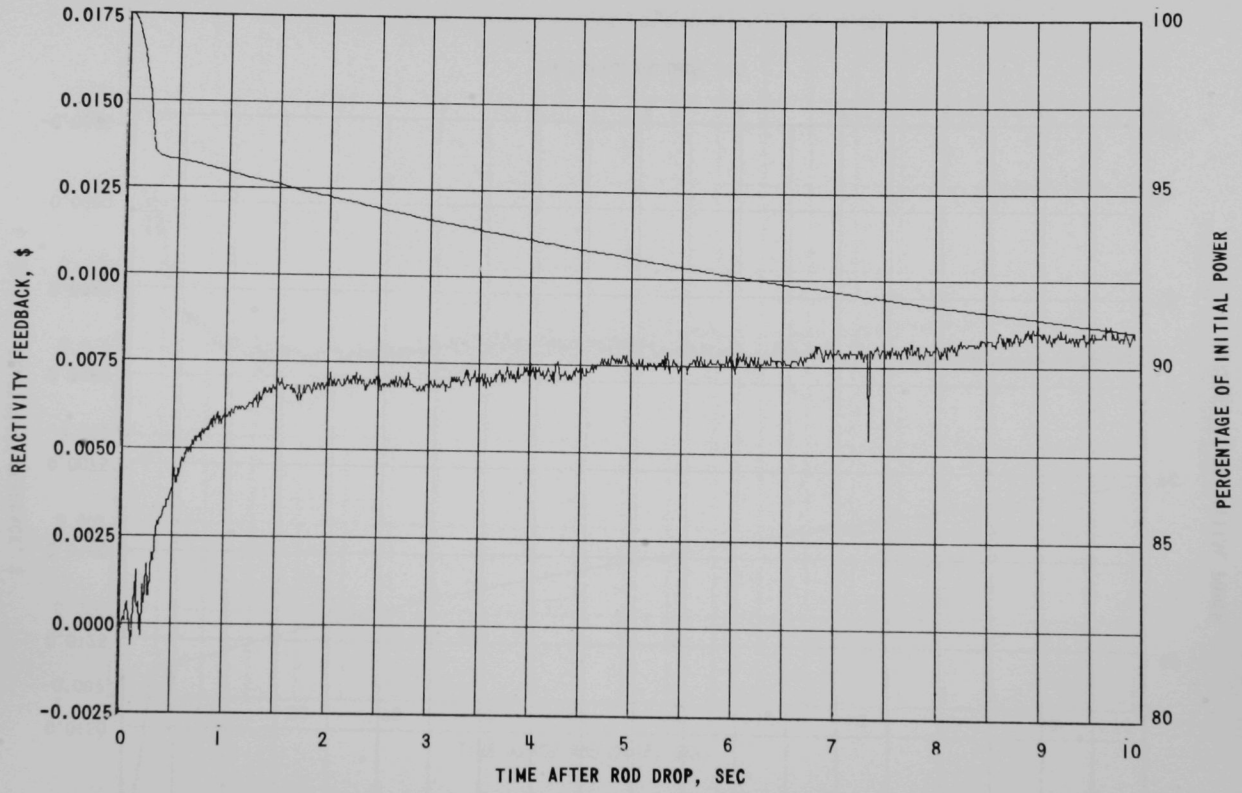

Fig. 18. Rod-drop Results for Run 26A, 35.0 MWt, Full Flow (9-26-67)

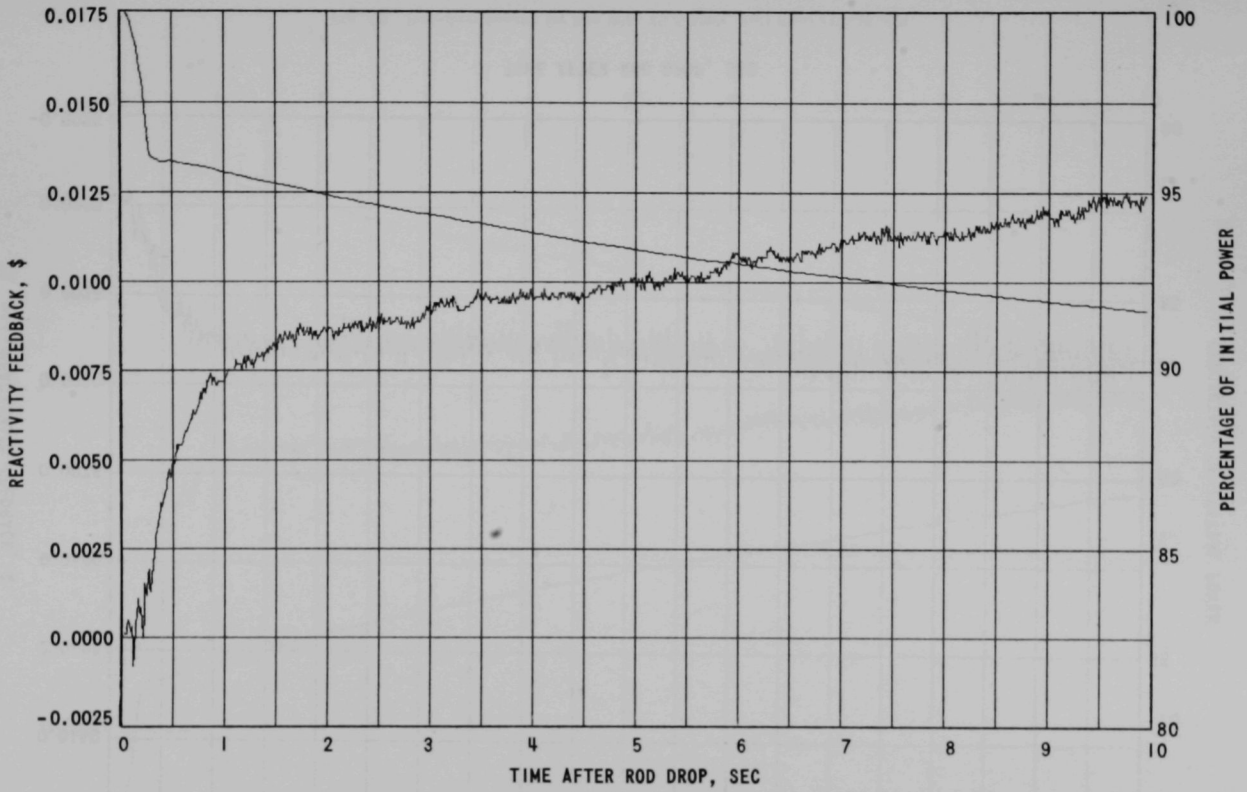

Fig. 19. Rod-drop Results for Run 26A, 45 MWt, 13-in. Bank Full Flow (9-26-67)

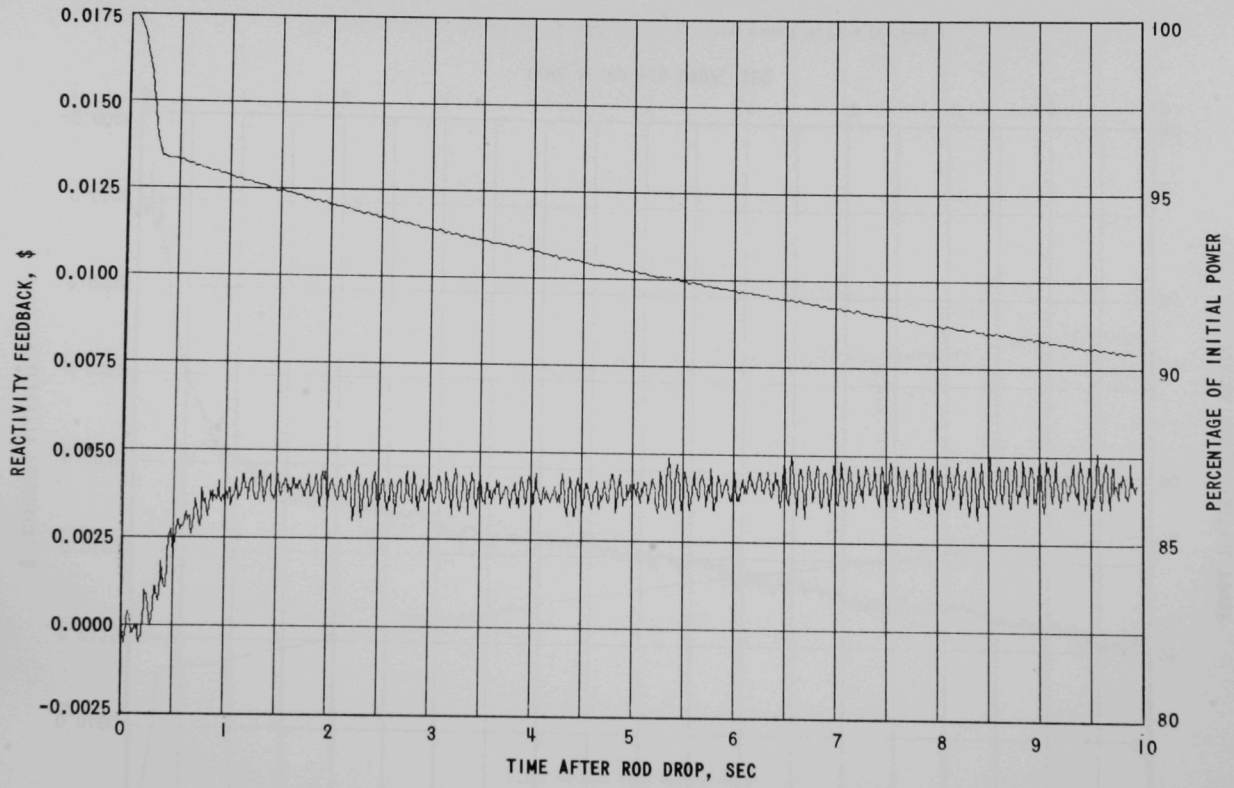

Fig. 20. Rod-drop Results for Run 26B, 22.5 MWt, Full Flow (10-16-67)

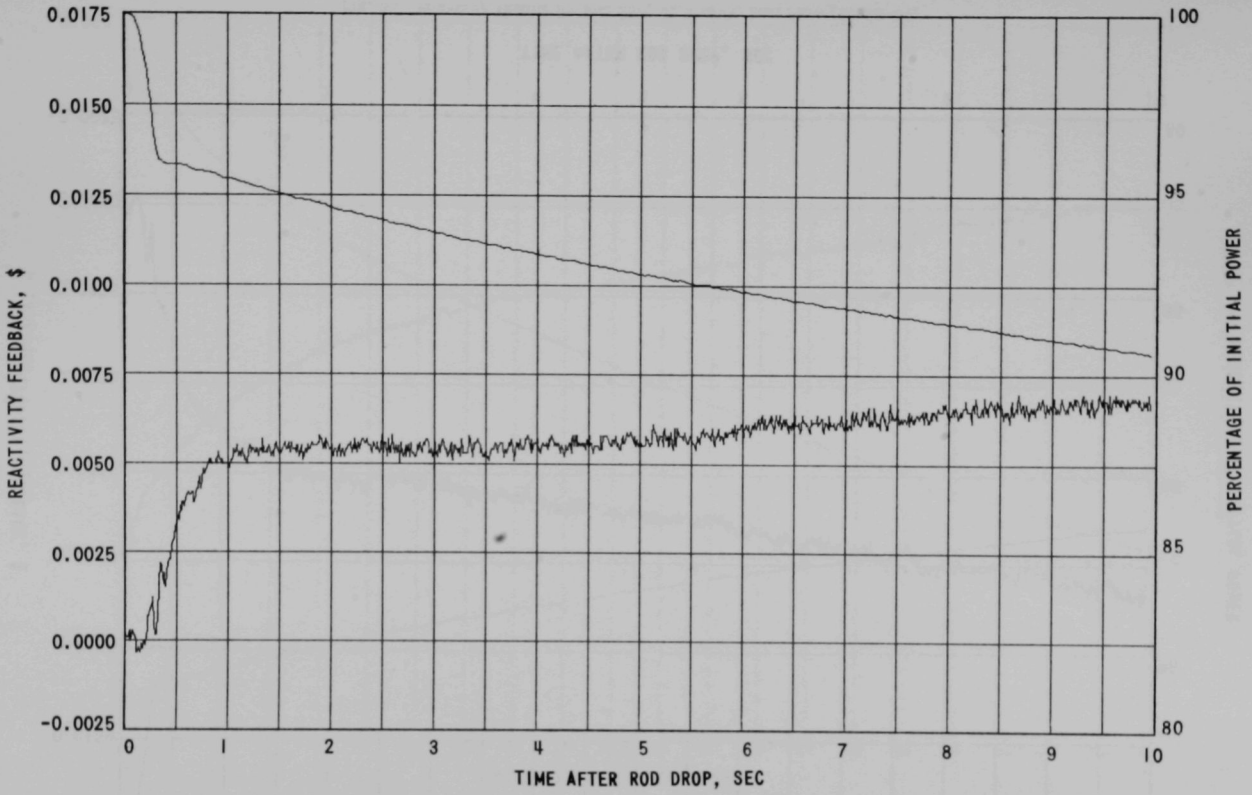

Fig. 21. Rod-drop Results for Run 26B, 30 MWt, Full Flow (10-17-67)

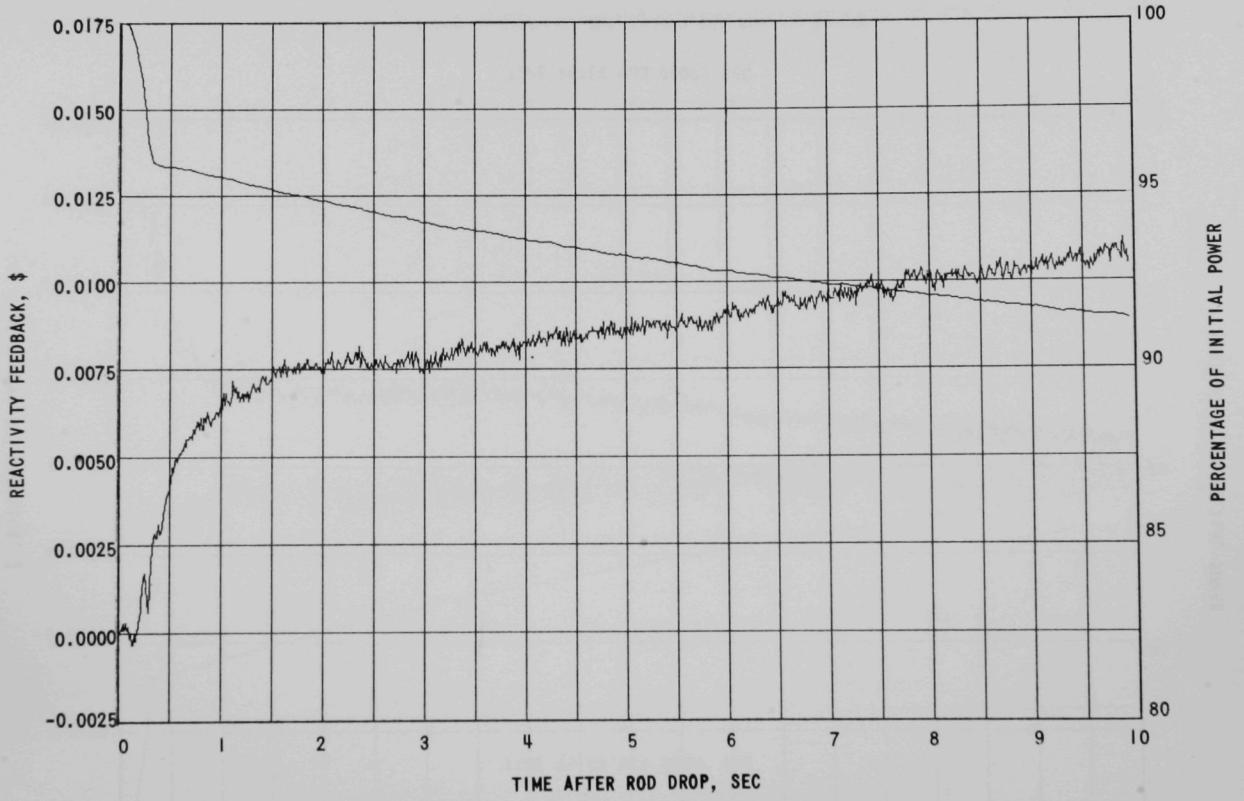

Fig. 22. Rod-drop Results for Run 26B, 41.5 MWt, Full Flow (10-18-67)

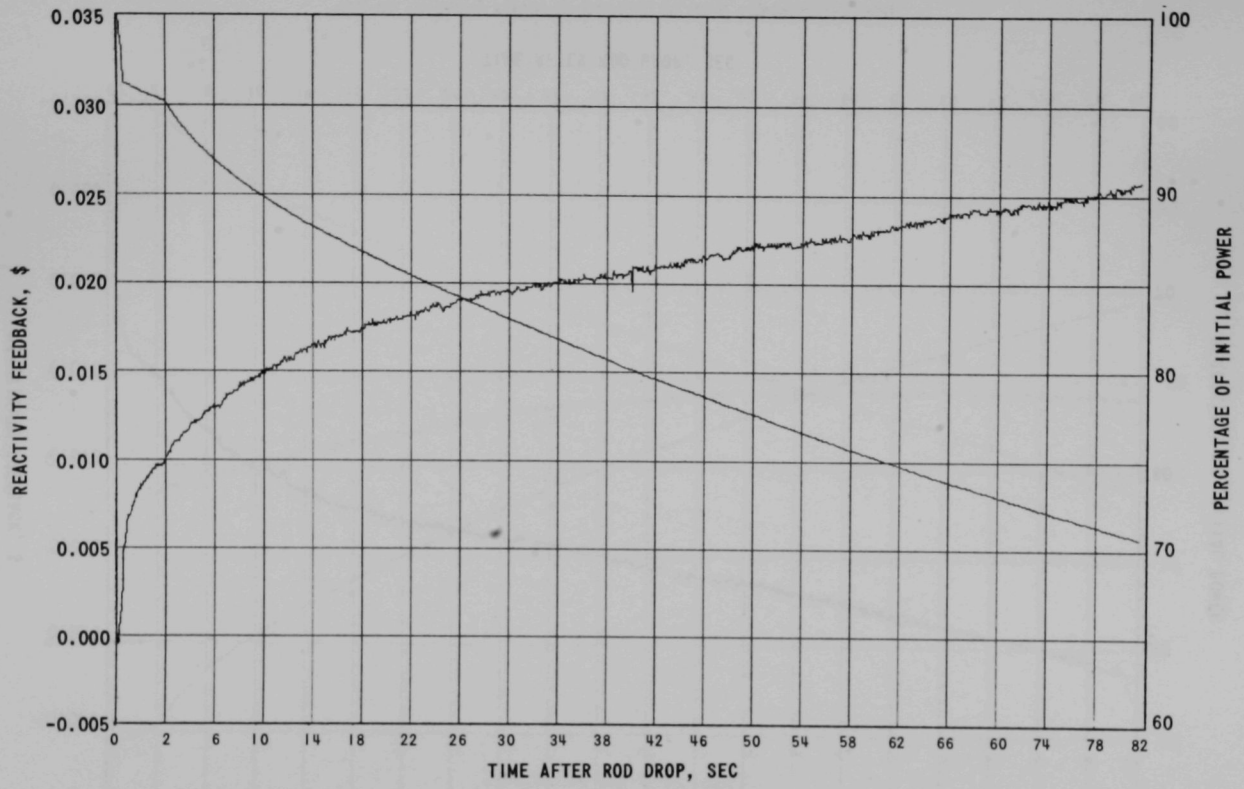

Fig. 23. Rod-drop Results for Run 27C, 22.5 MWt, 54% Flow (3-9-68)

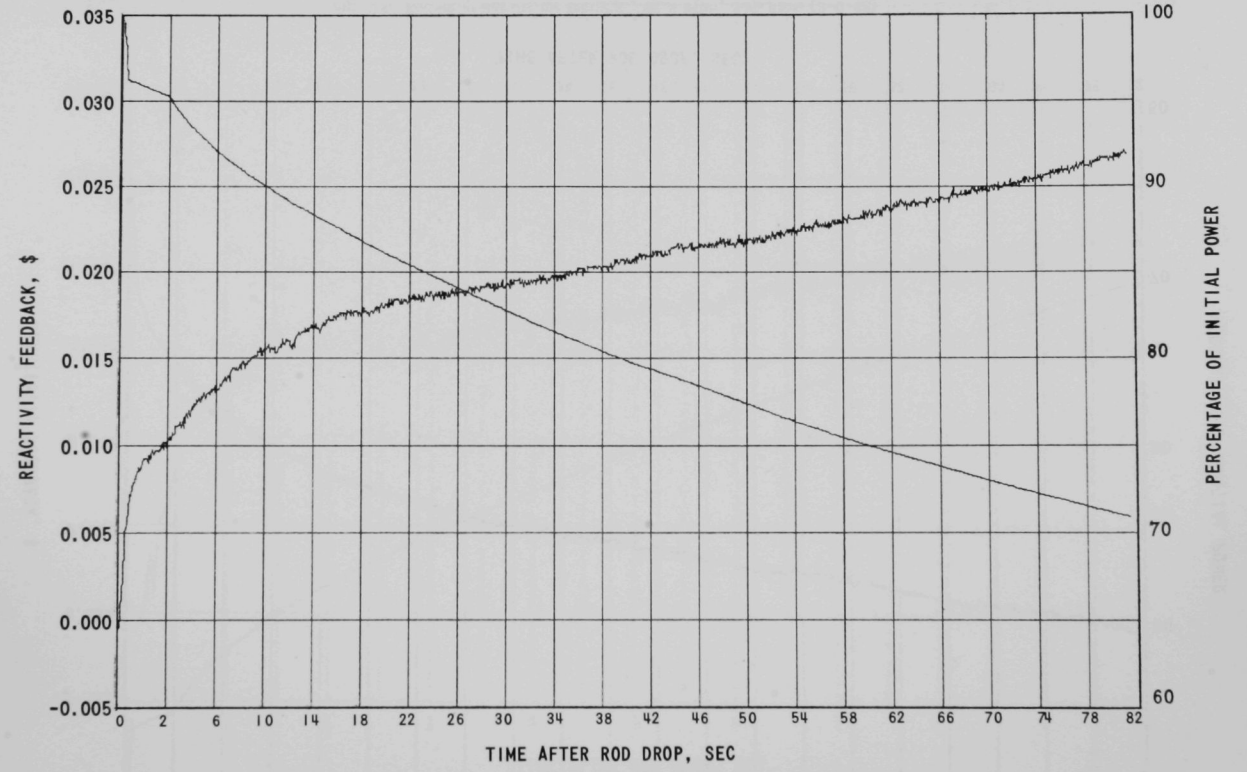

Fig. 24. Rod-drop Results for Run 27C, 30 MWt, 75% Flow (3-11-68)

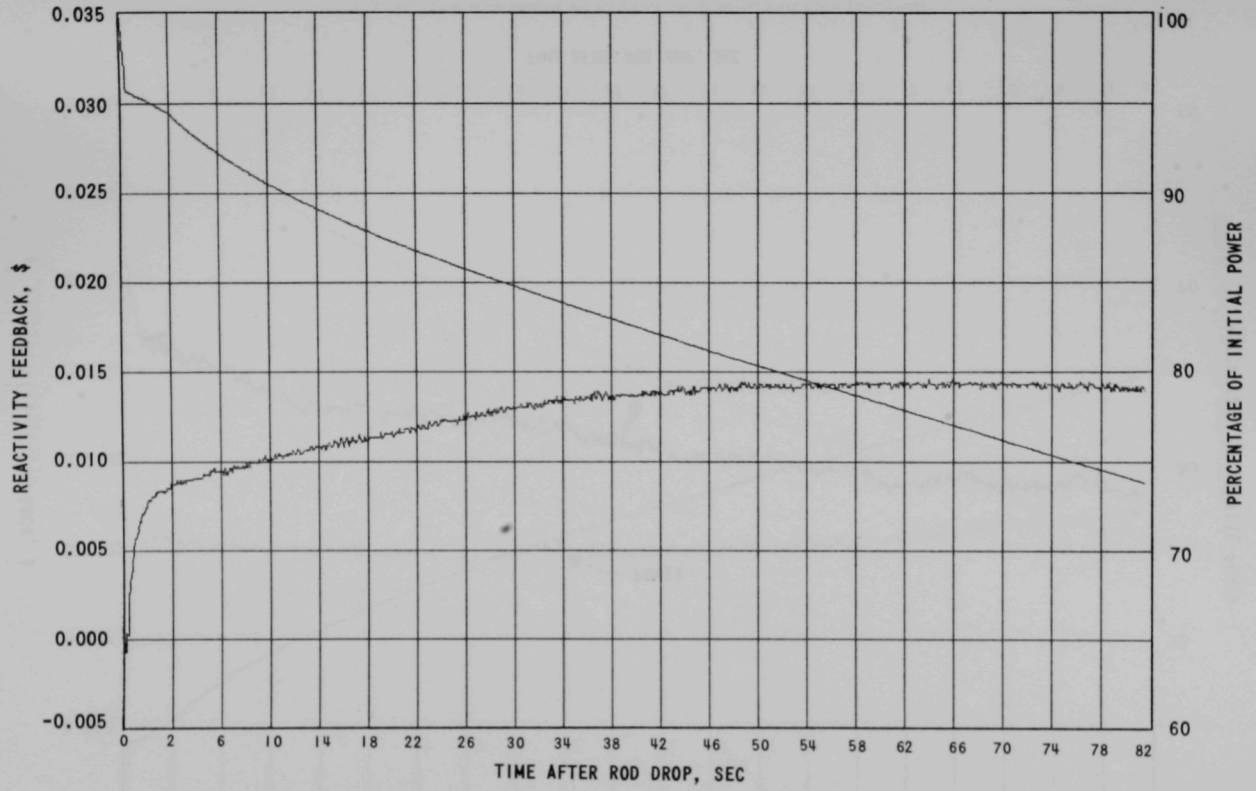

Fig. 25. Rod-drop Results for Run 28A, 22.5 MWt, 54% Flow (5-10-68)

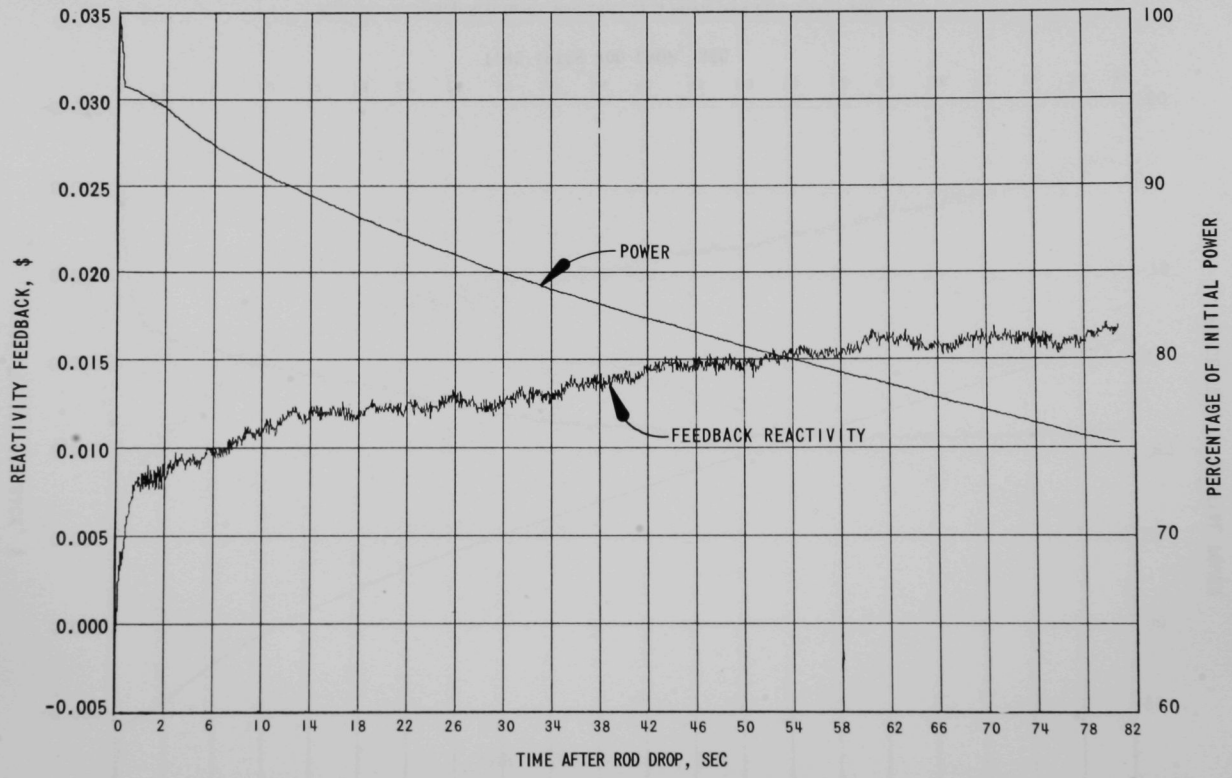

Fig. 26. Rod-drop Results for Run 28A, 41.5 MWt, Full Flow (5-10-68)

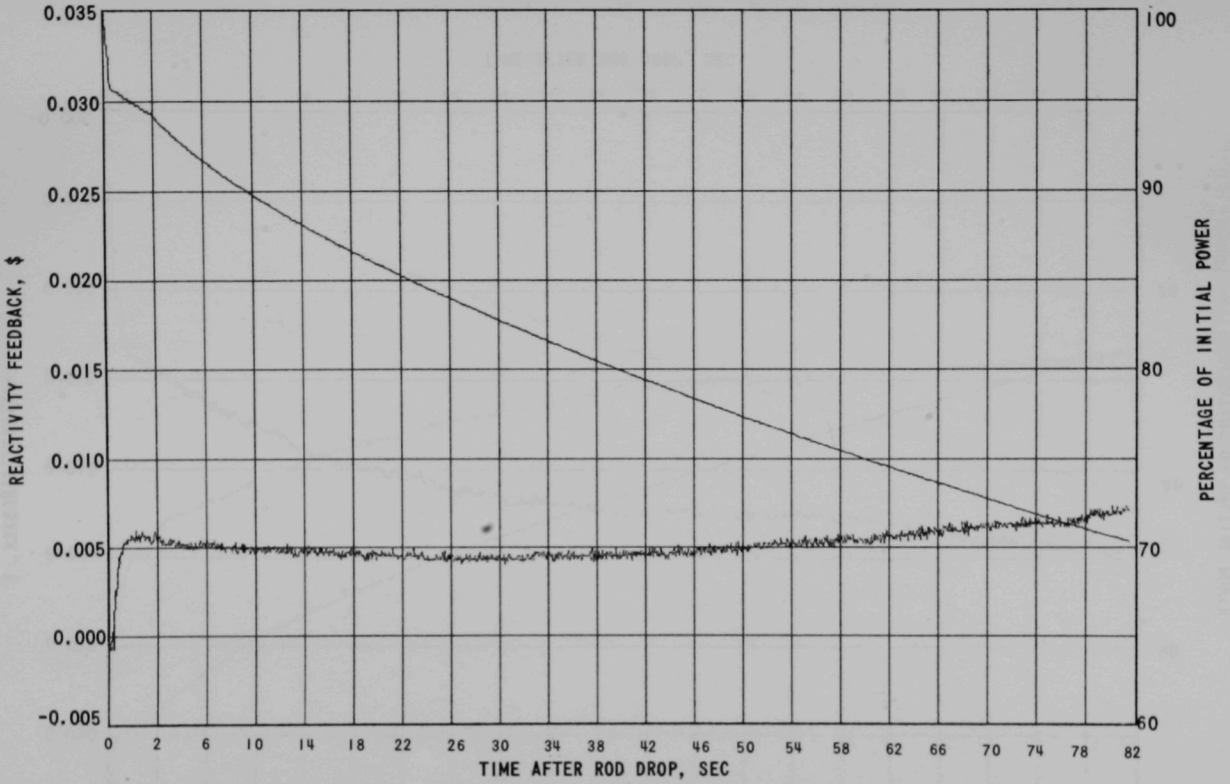

Fig. 27. Rod-drop Results for Run 28A, 22.5 MWt, Full Flow (5-13-68)

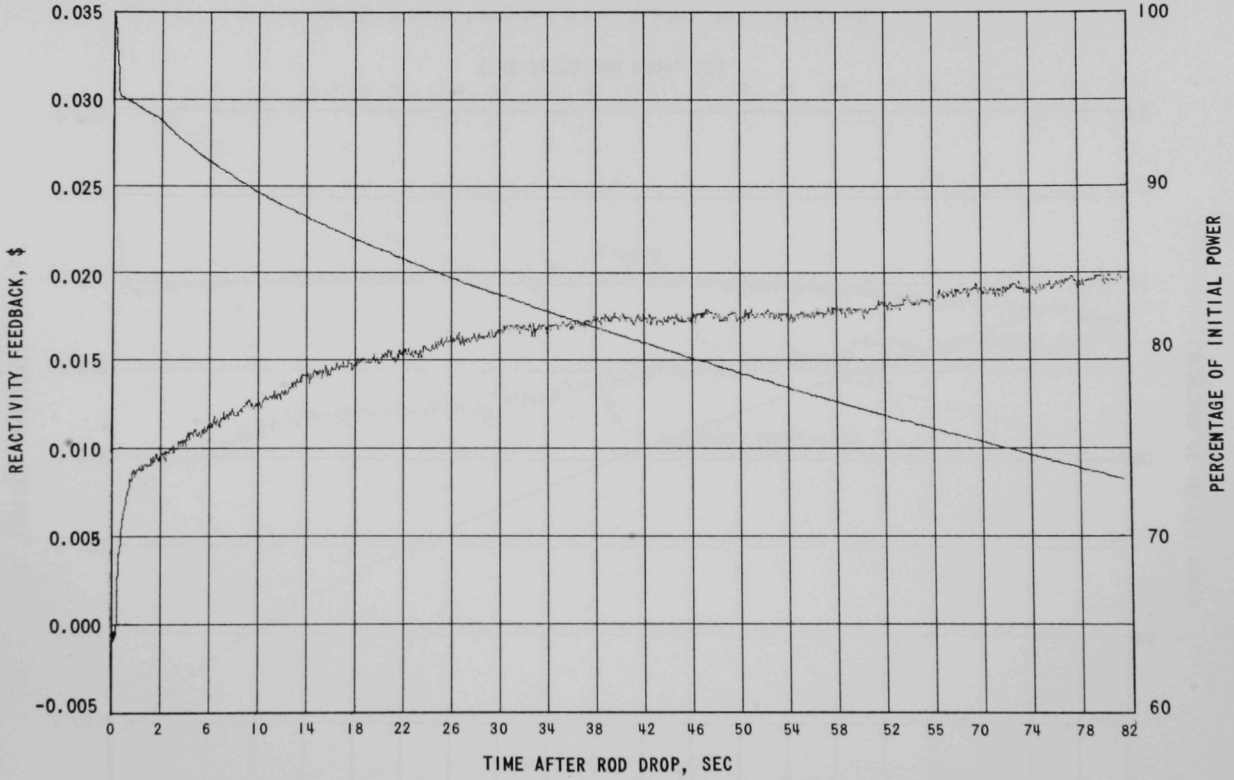

Fig. 28. Rod-drop Results for Run 28B, 41.5 MWt, Full Flow (5-20-68)

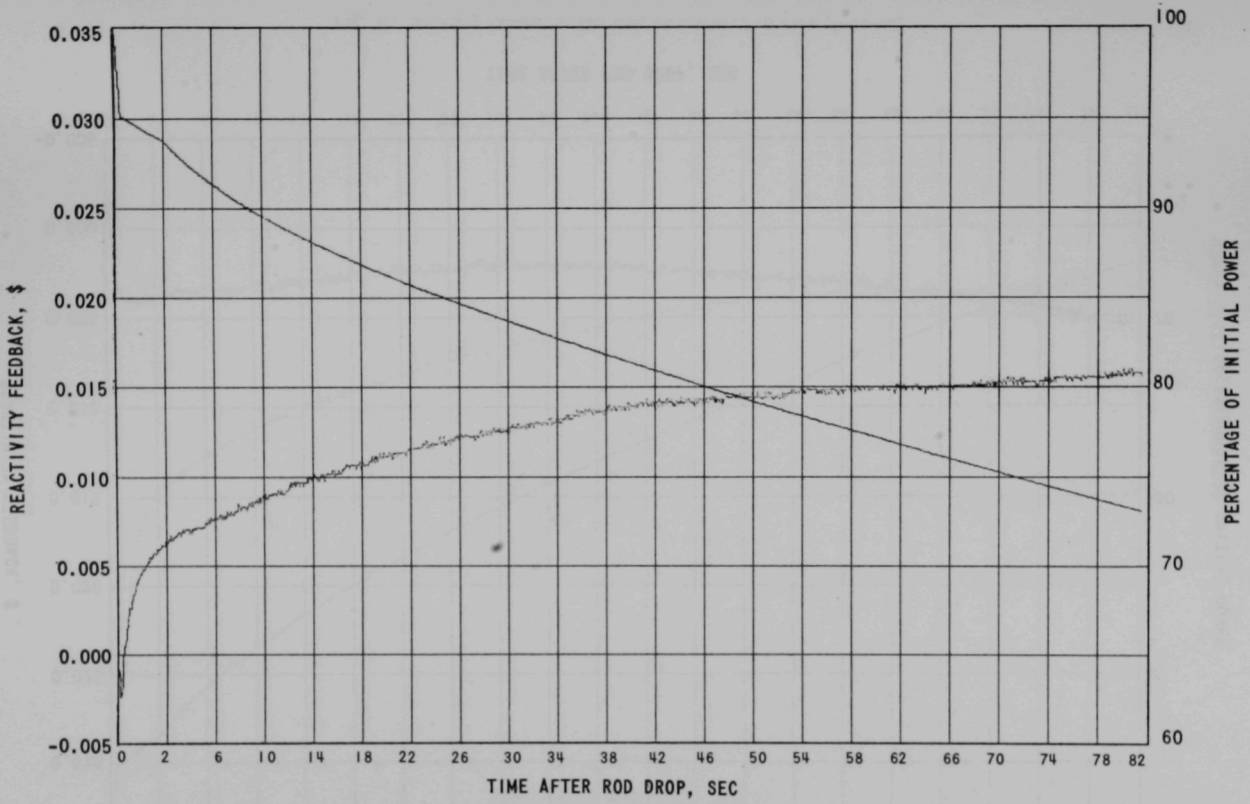

Fig. 29. Rod-drop Results for Run 28B, 22.5 MWt, 54% Flow (5-22-68)

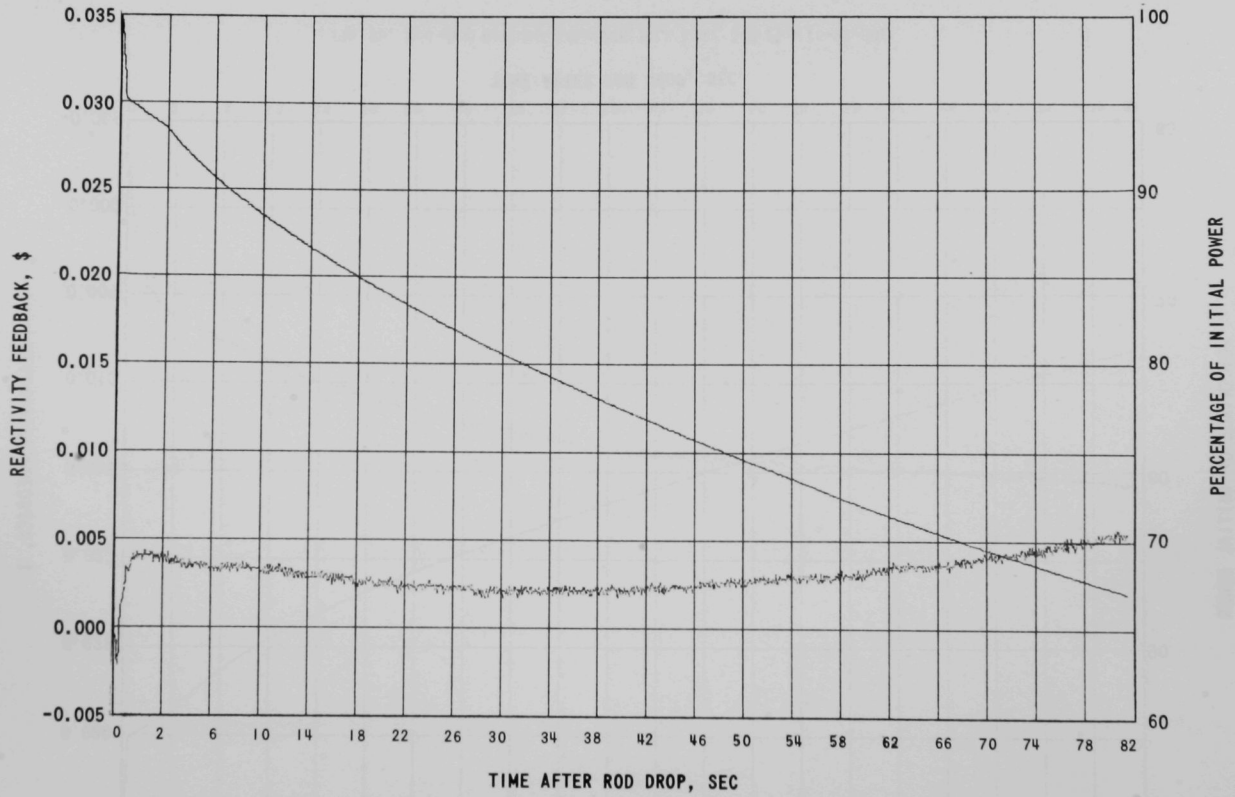

Fig. 30. Rod-drop Results for Run 28B, 22.5 MWt, Full Flow (5-24-68)

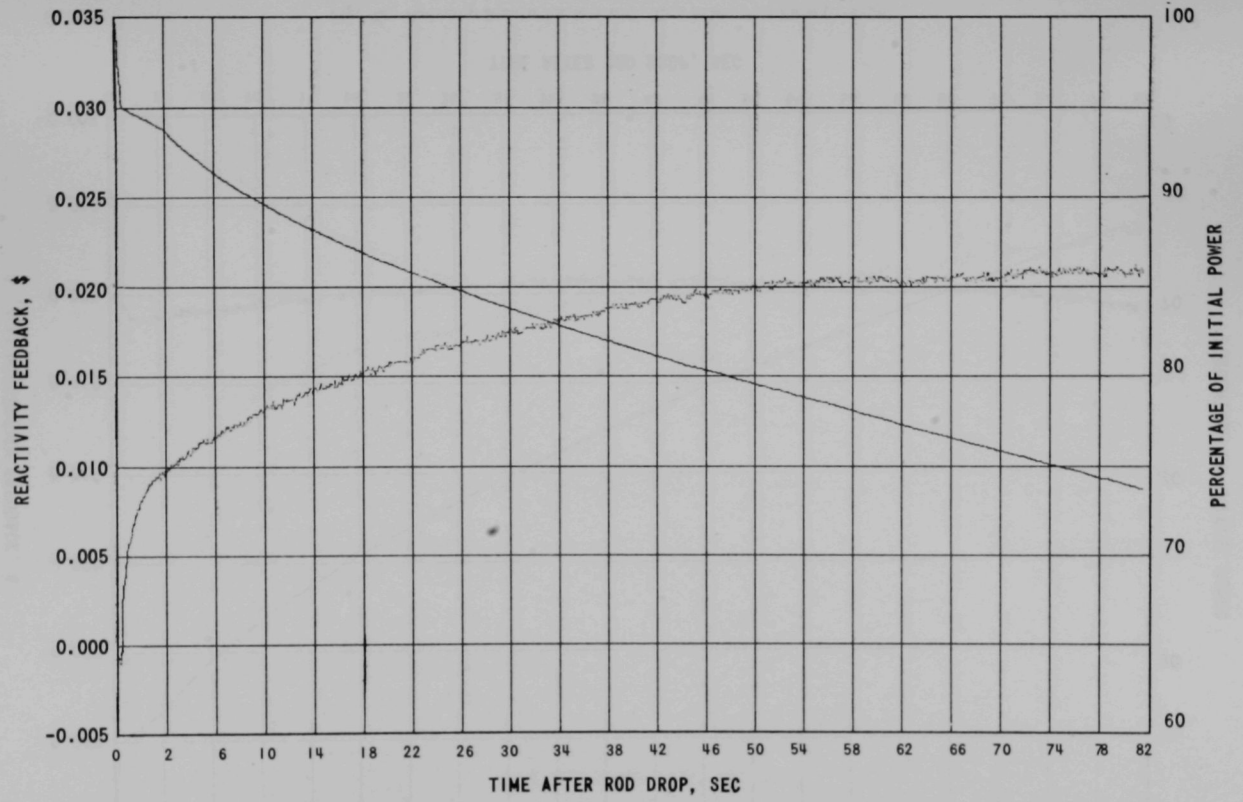

Fig. 31. Rod-drop Results for Run 28C, 22.5 MWt, 58% Flow (6-3-68)

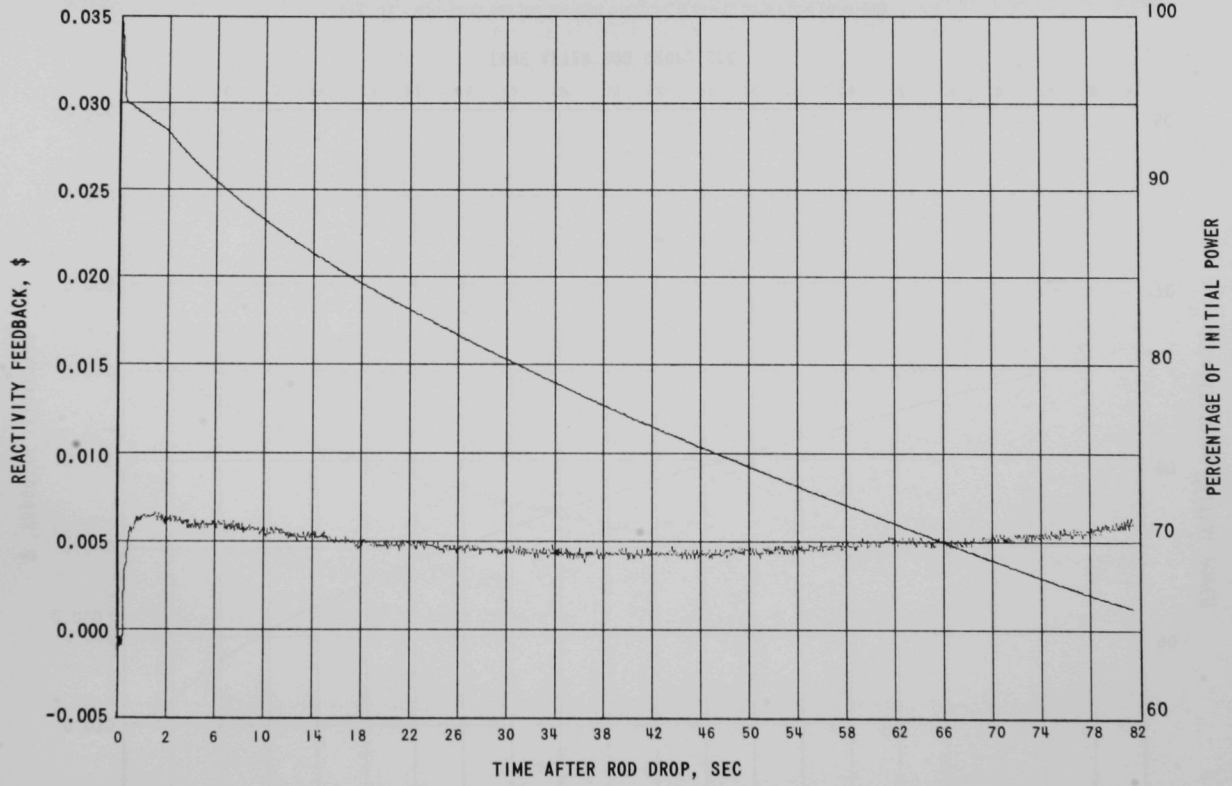

Fig. 32. Rod-drop Results for Run 28C, 22.5 MWt, Full Flow (6-4-68)

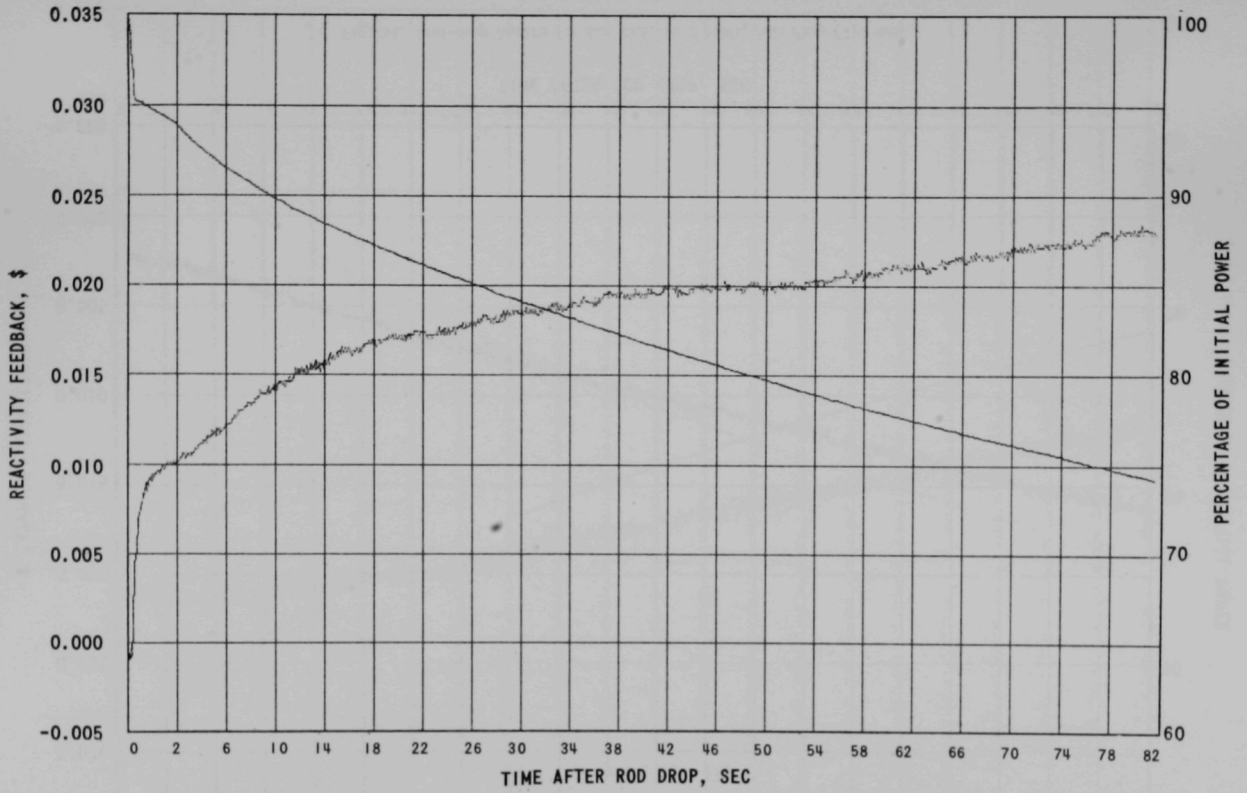

Fig. 33. Rod-drop Results for Run 28C, 41.5 MWt, Full Flow (6-4-68)

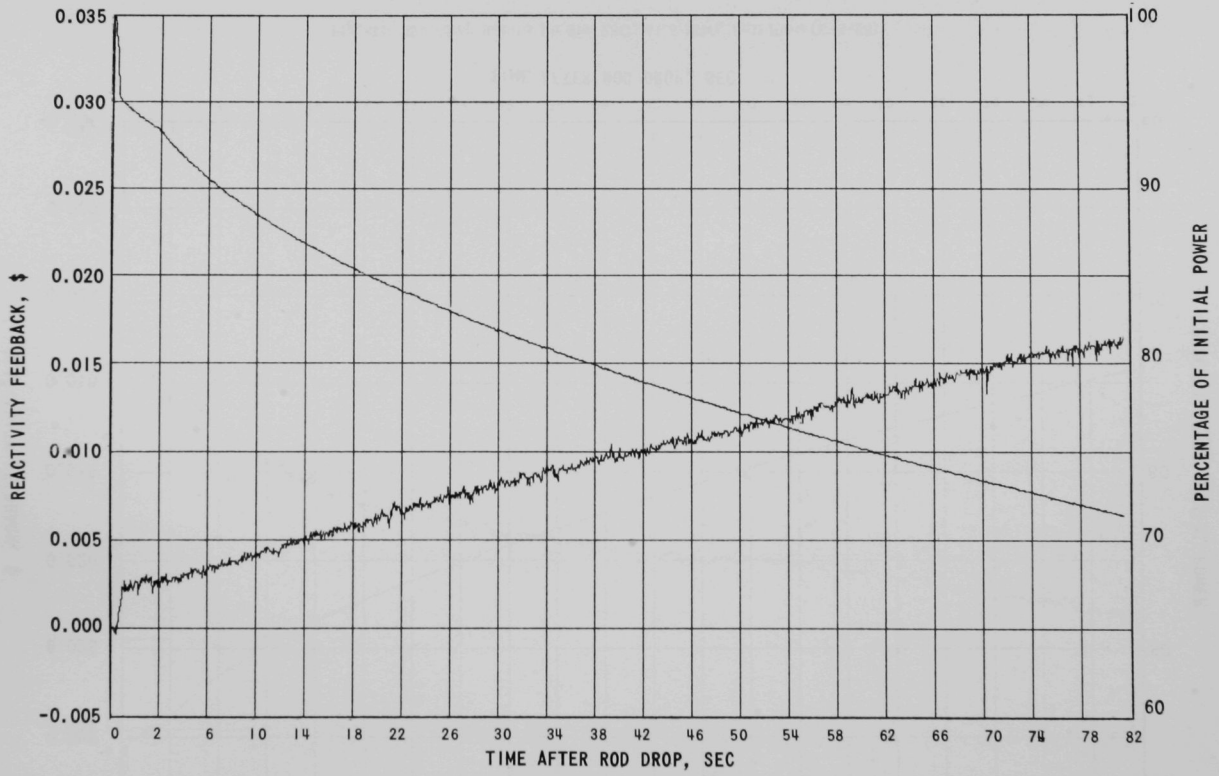

Fig. 34. Rod-drop Results for Run 29A, 12.5 MWt, Full Flow (7-1-68)

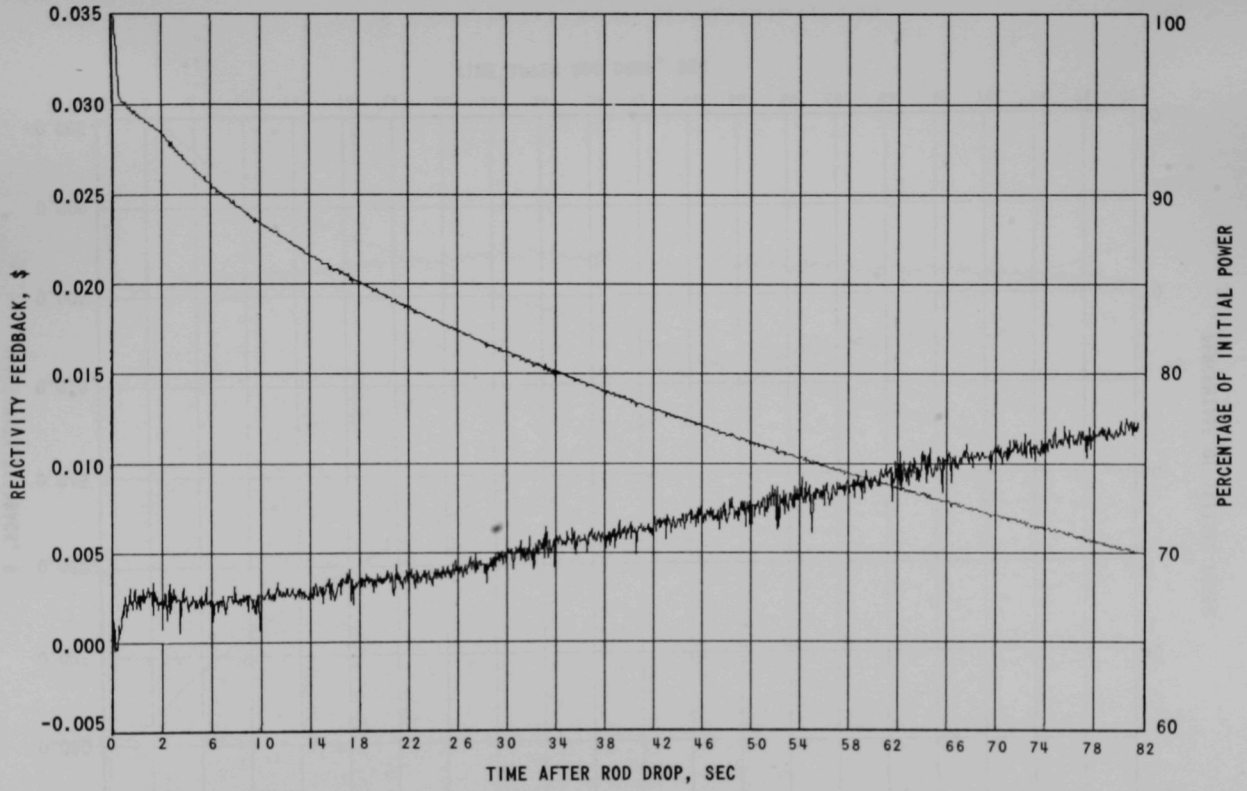

Fig. 35. Rod-drop Results for Run 29A, 15 MWt, Full Flow (7-1-68)

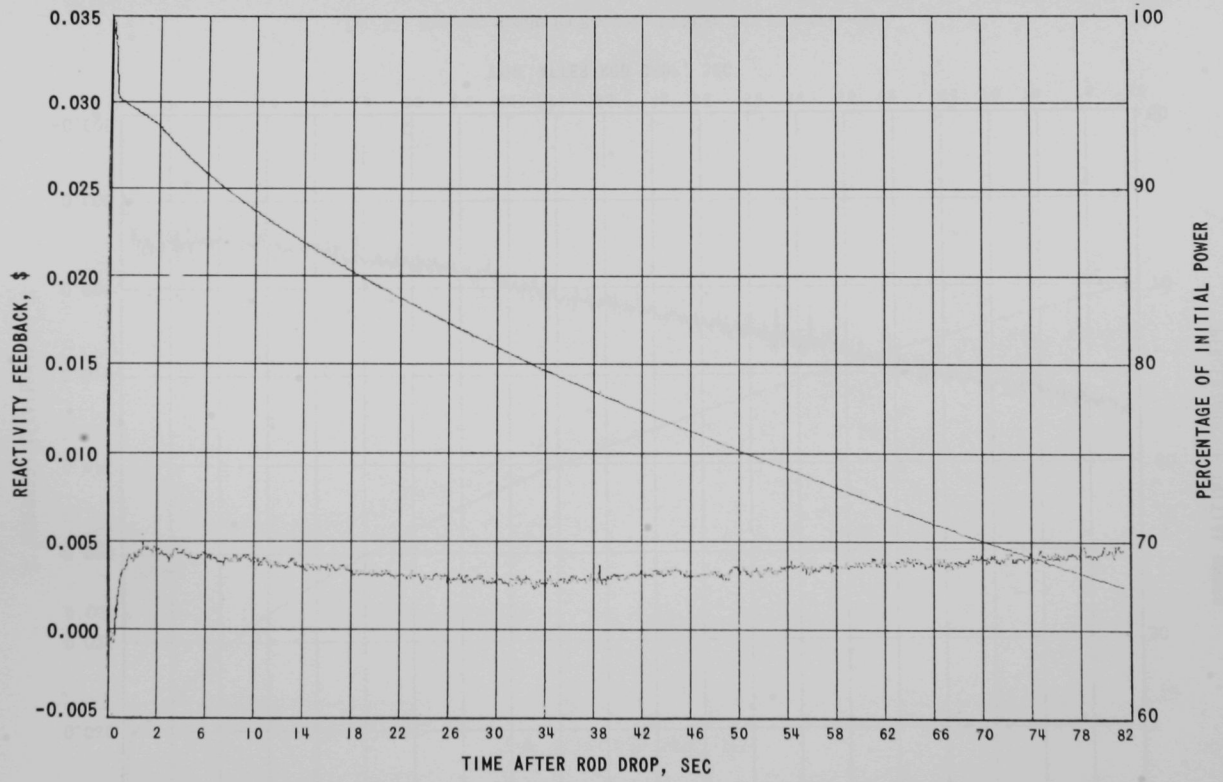

Fig. 36. Rod-drop Results for Run 29A, 25 MWt, Full Flow (7-1-68)

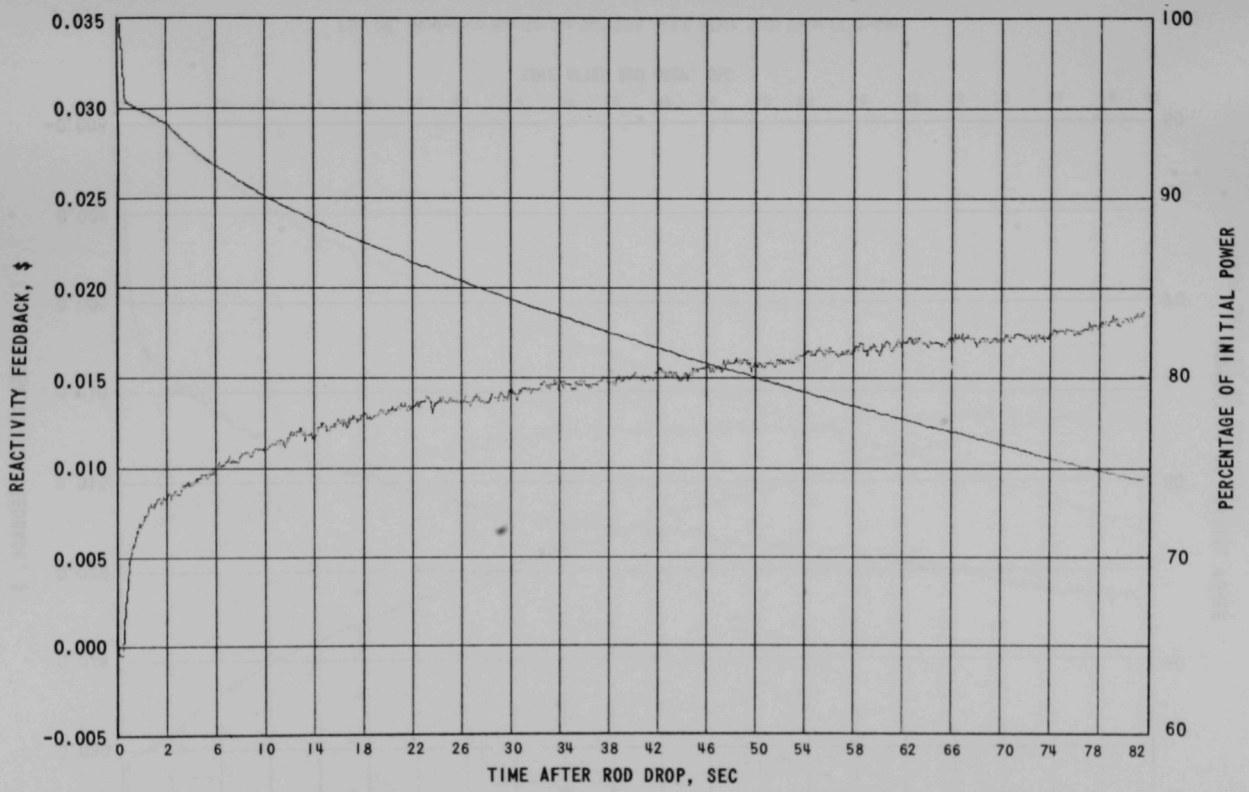

Fig. 37. Rod-drop Results for Run 29A, 41.5 MWt, Full Flow (7-1-68)

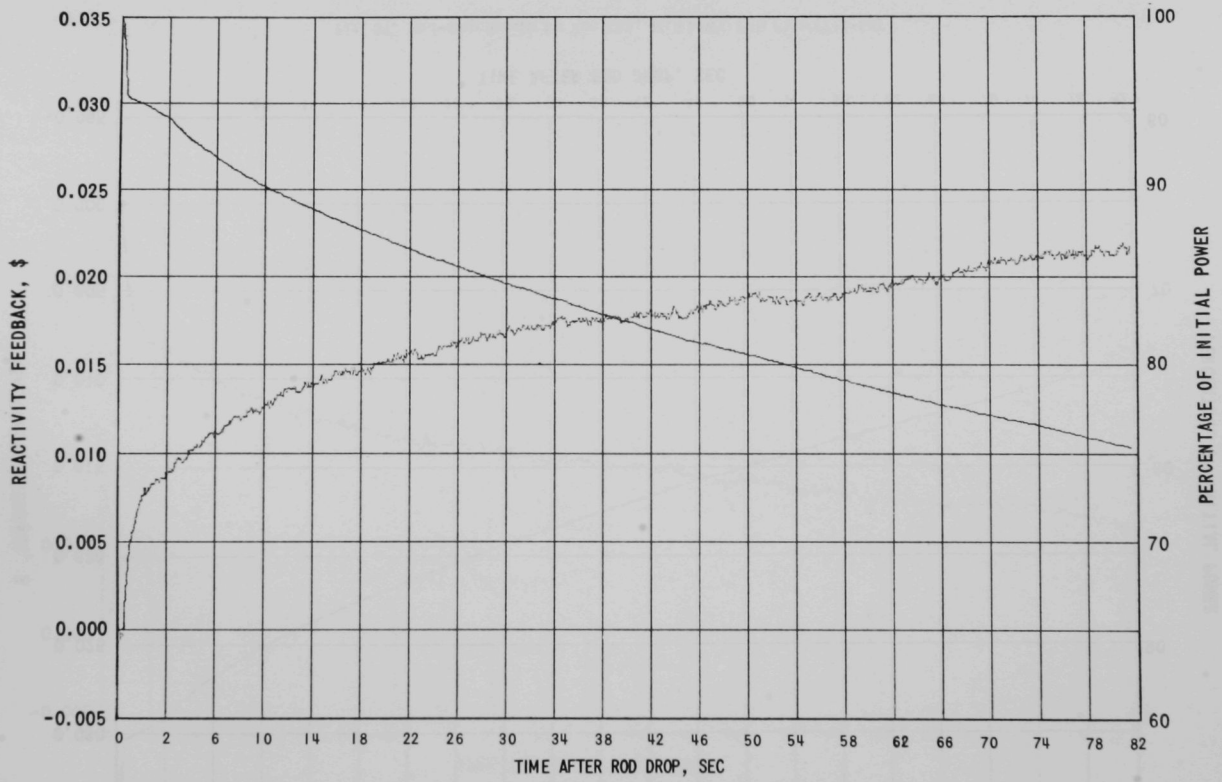

Fig. 38. Rod-drop Results for Run 29A, 45.0 MWt, Full Flow (7-1-68)

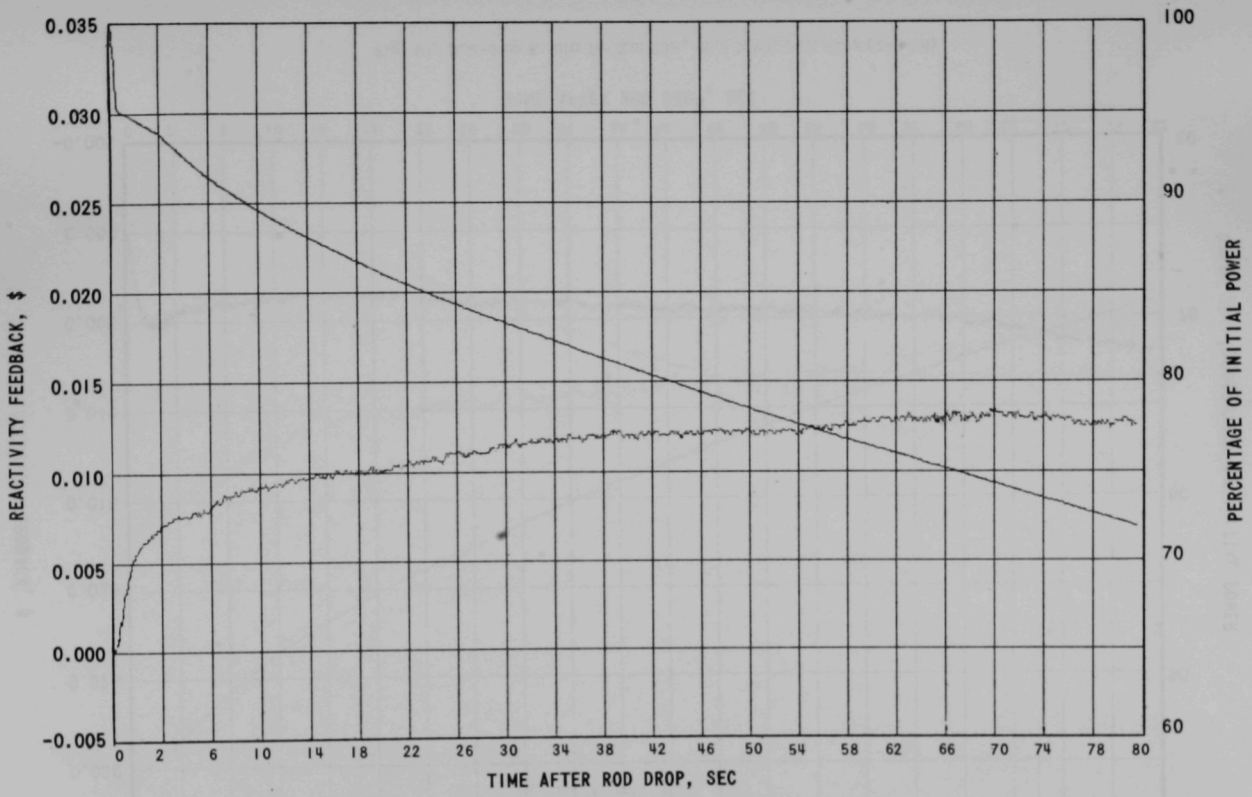

Fig. 39. Rod-drop Results for Run 29A, 22.5 MWt, 58% Flow (7-2-68)

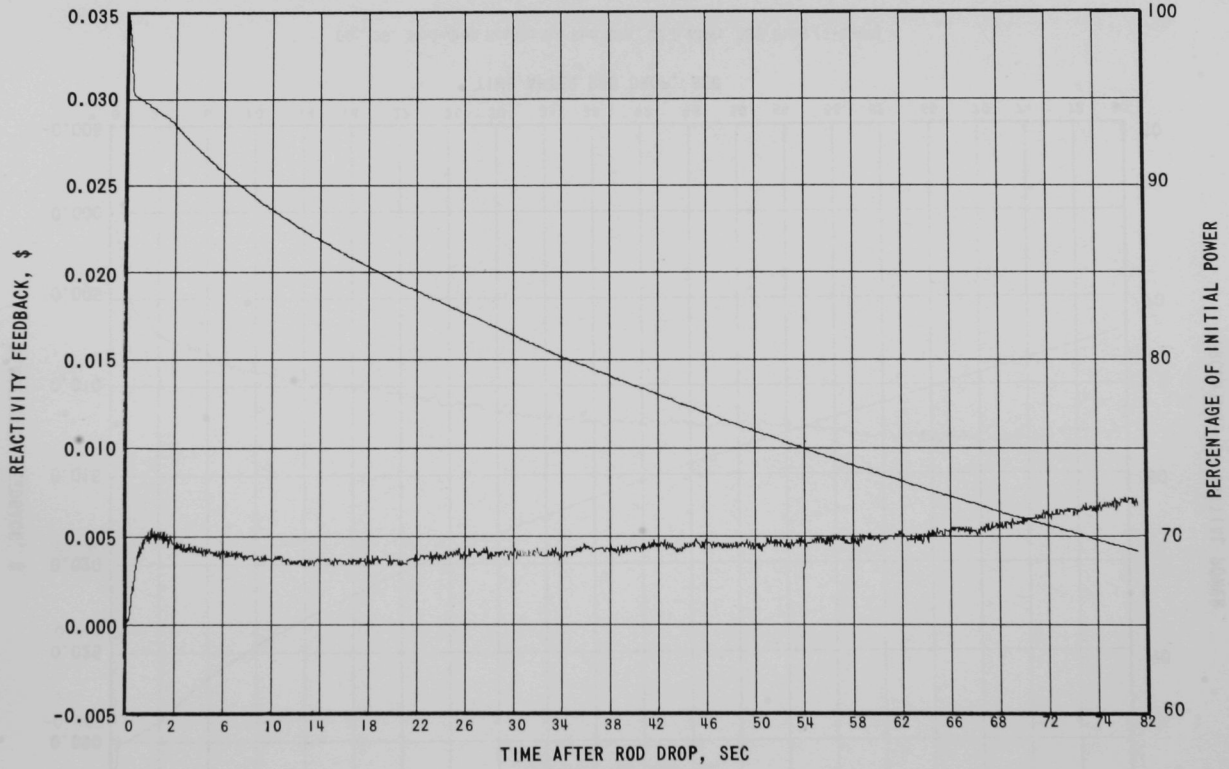

Fig. 40. Rod-drop Results for Run 29A, 22.5 MWt, Full Flow (7-3-68)

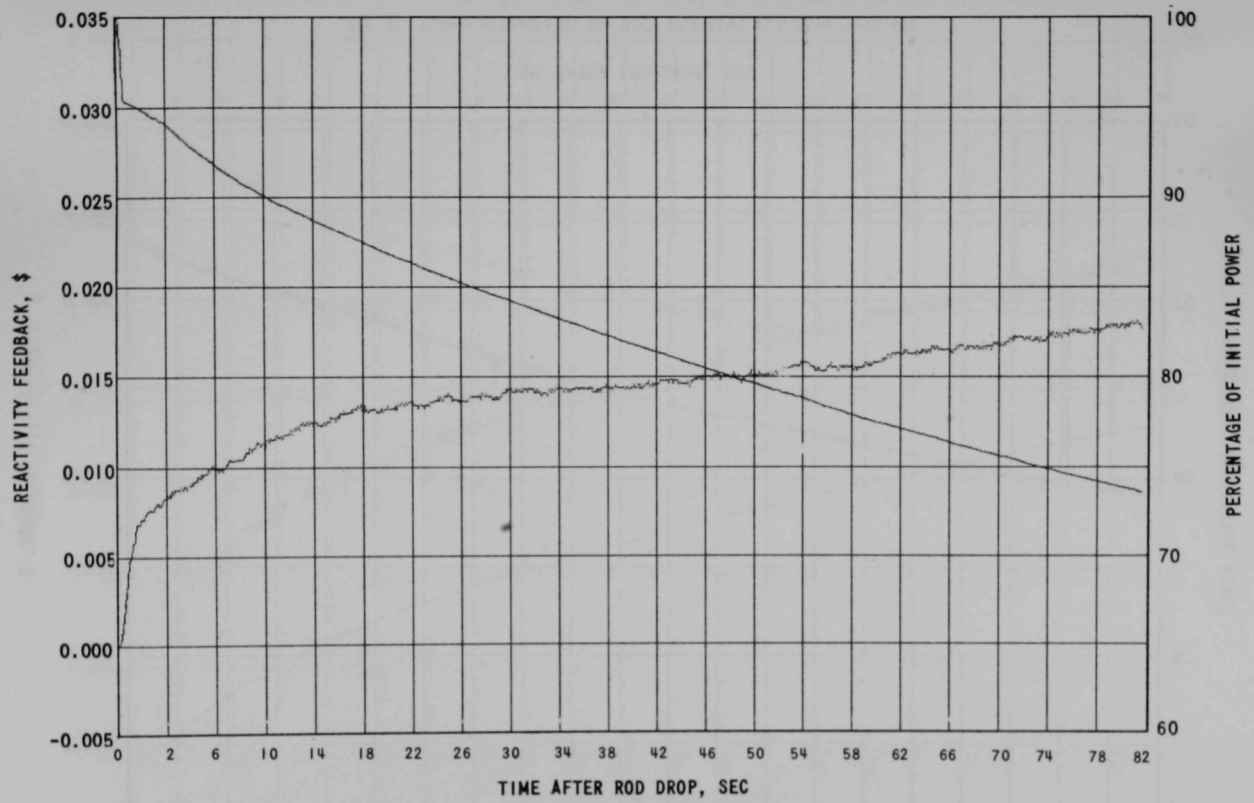

Fig. 41. Rod-drop Results for Run 29A, 41.5 MWt, Full Flow (7-3-68)

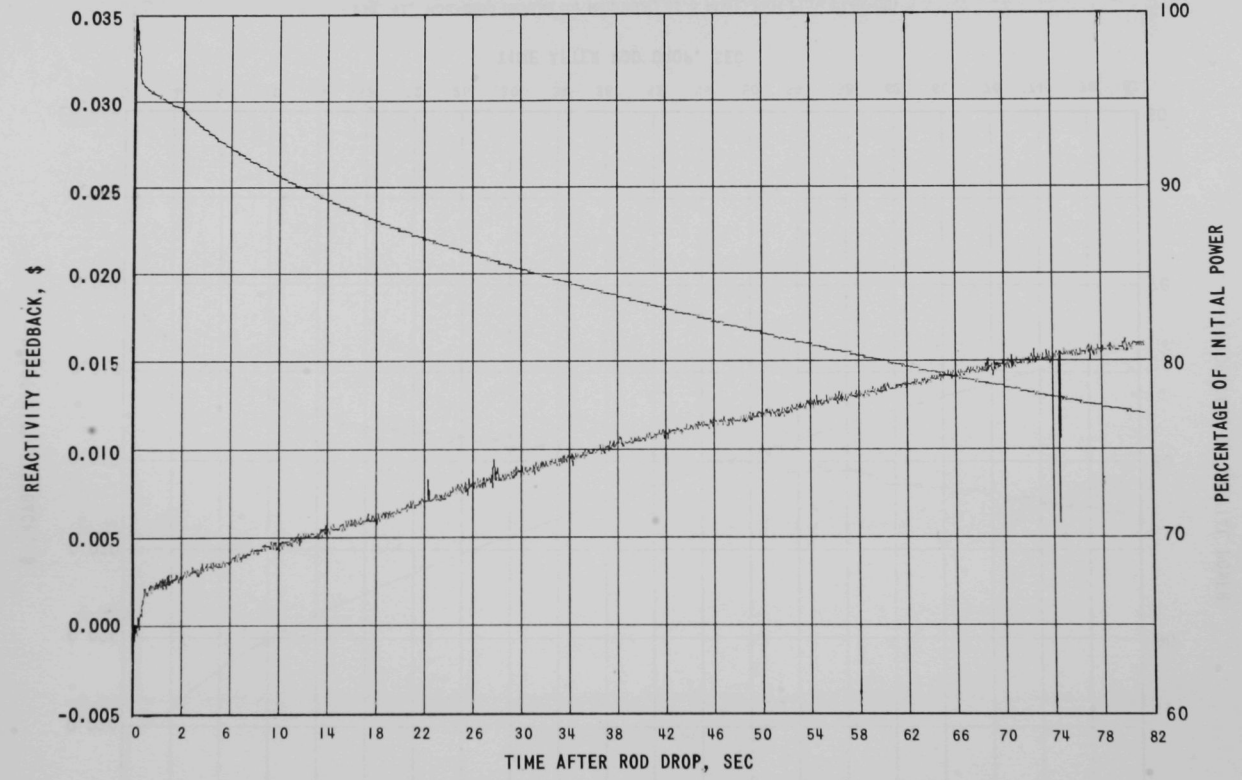

Fig. 42. Rod-drop Results for Run 29C, 12.5 MWt, Full Flow (7-18-68)

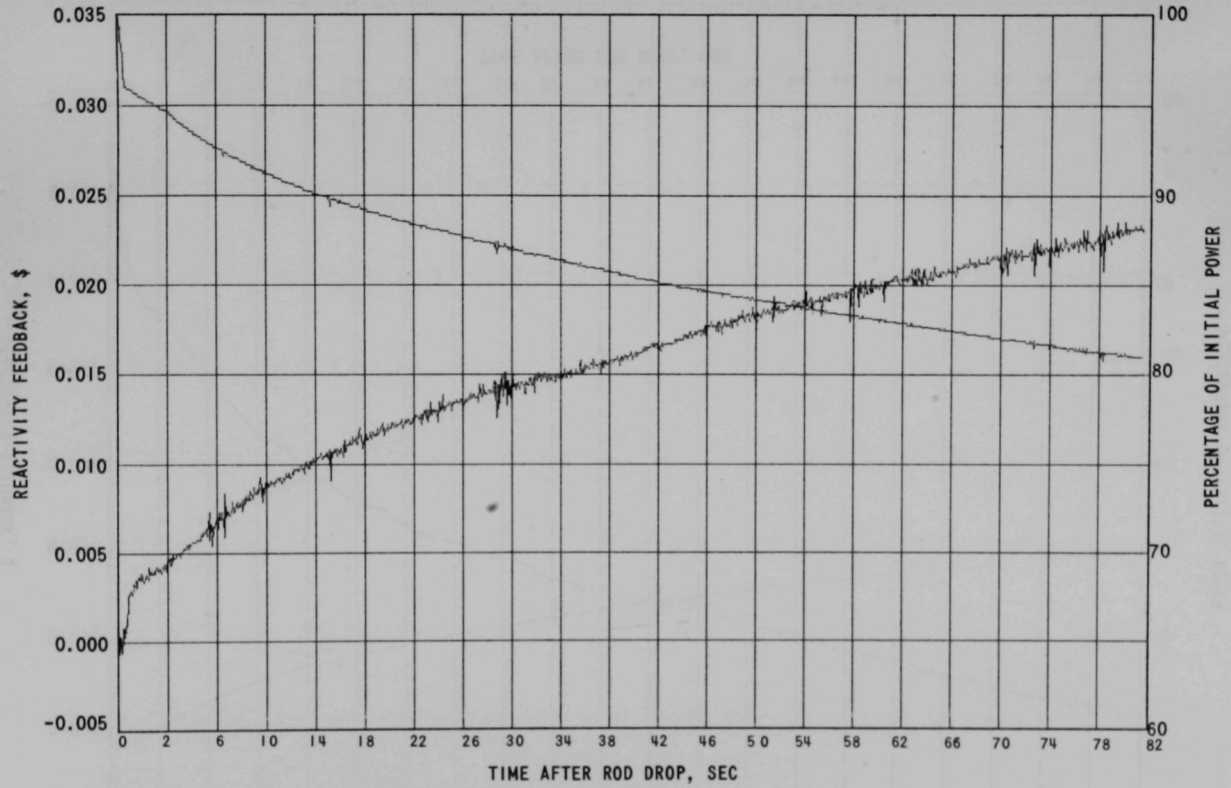

Fig. 43. Rod-drop Results for Run 29C, 25 MWt, Full Flow (7-18-68)

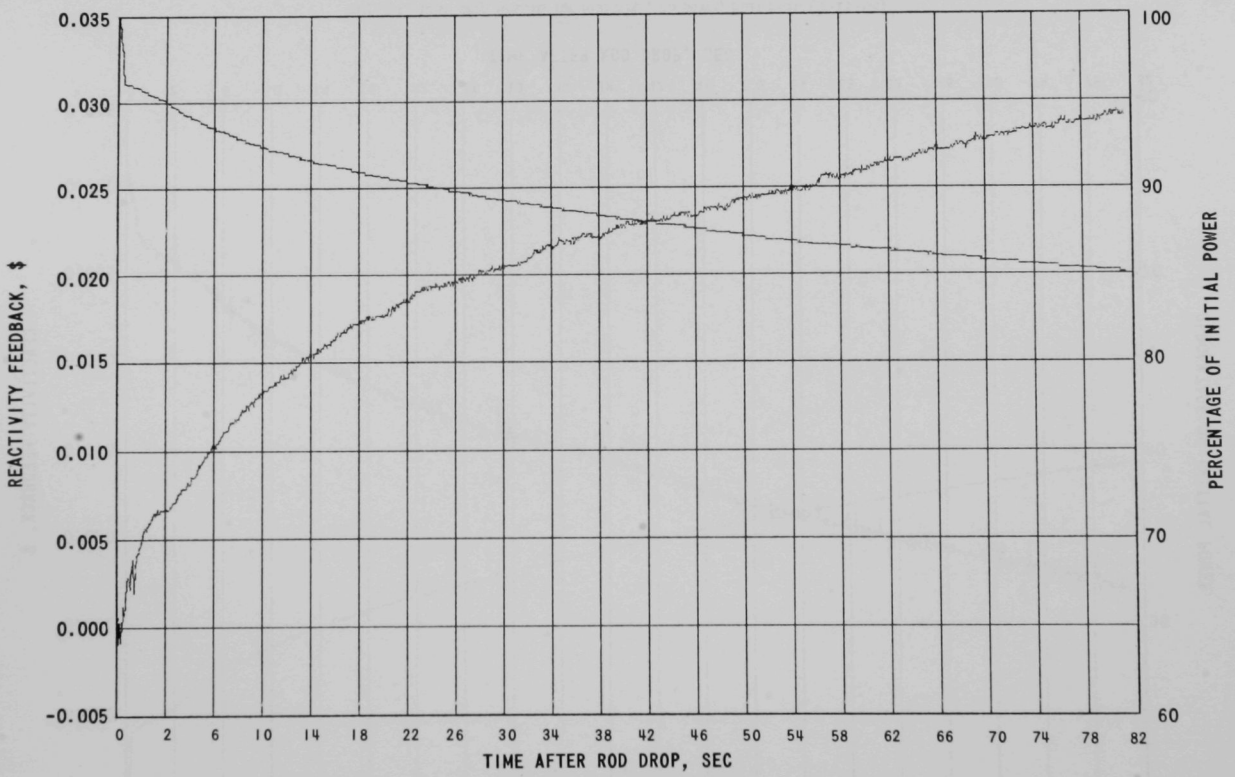

Fig. 44. Rod-drop Results for Run 29C, 41.5 MWt, Full Flow (7-18-68)

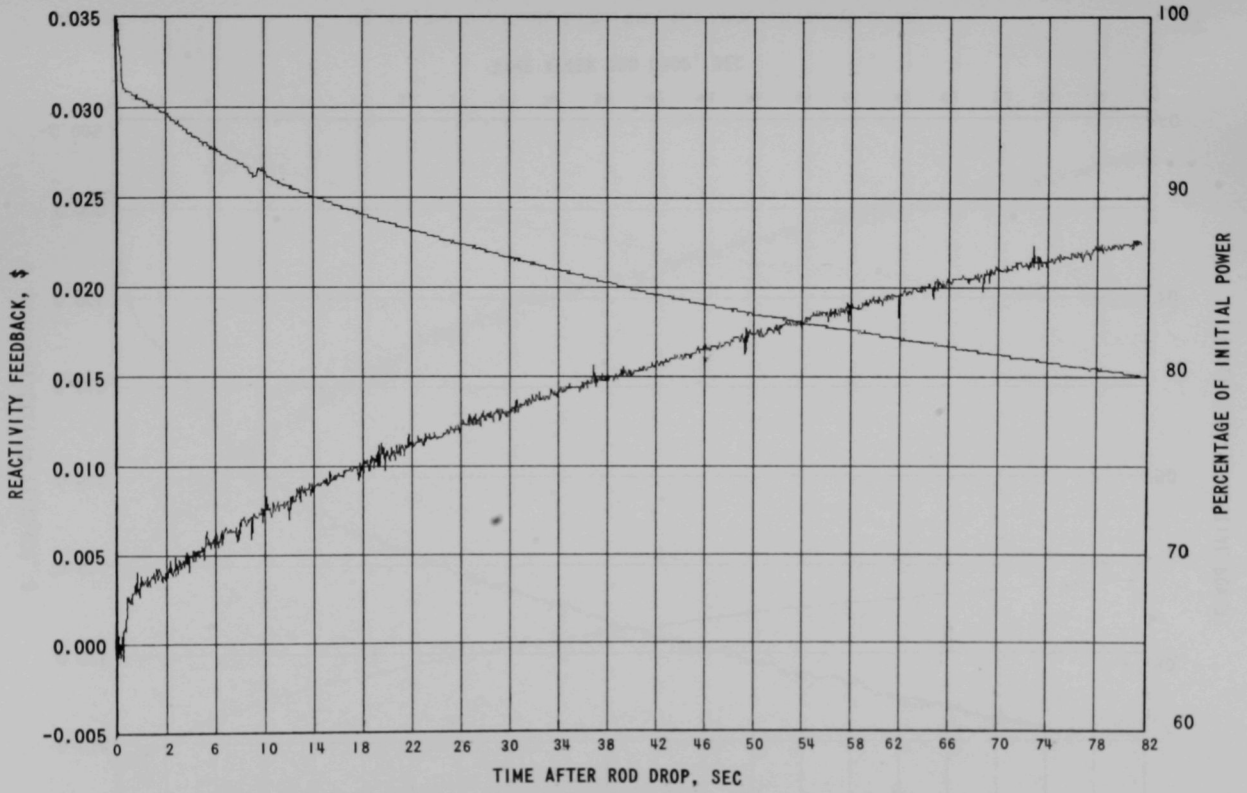

Fig. 45. Rod-drop Results for Run 29C, 22.5 MWt, Full Flow (7-19-68)

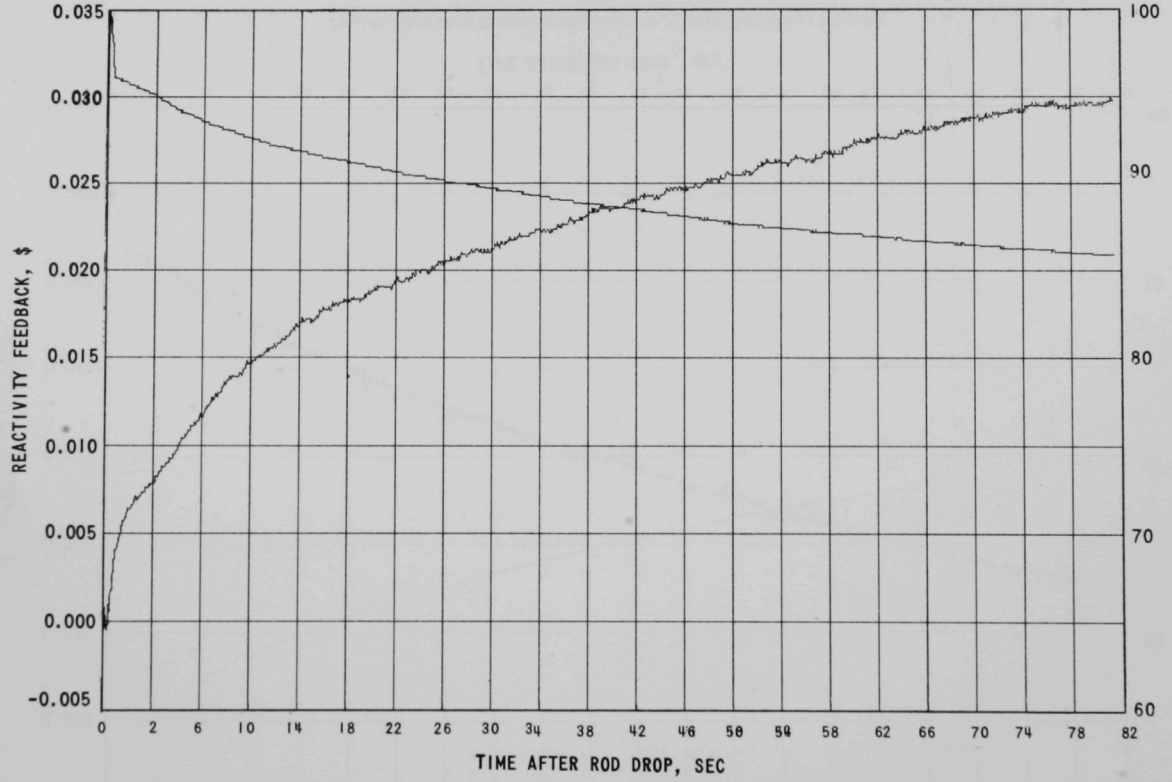

Fig. 46. Rod-drop Results for Run 29C, 45.0 MWt, Full Flow (7-18-68)

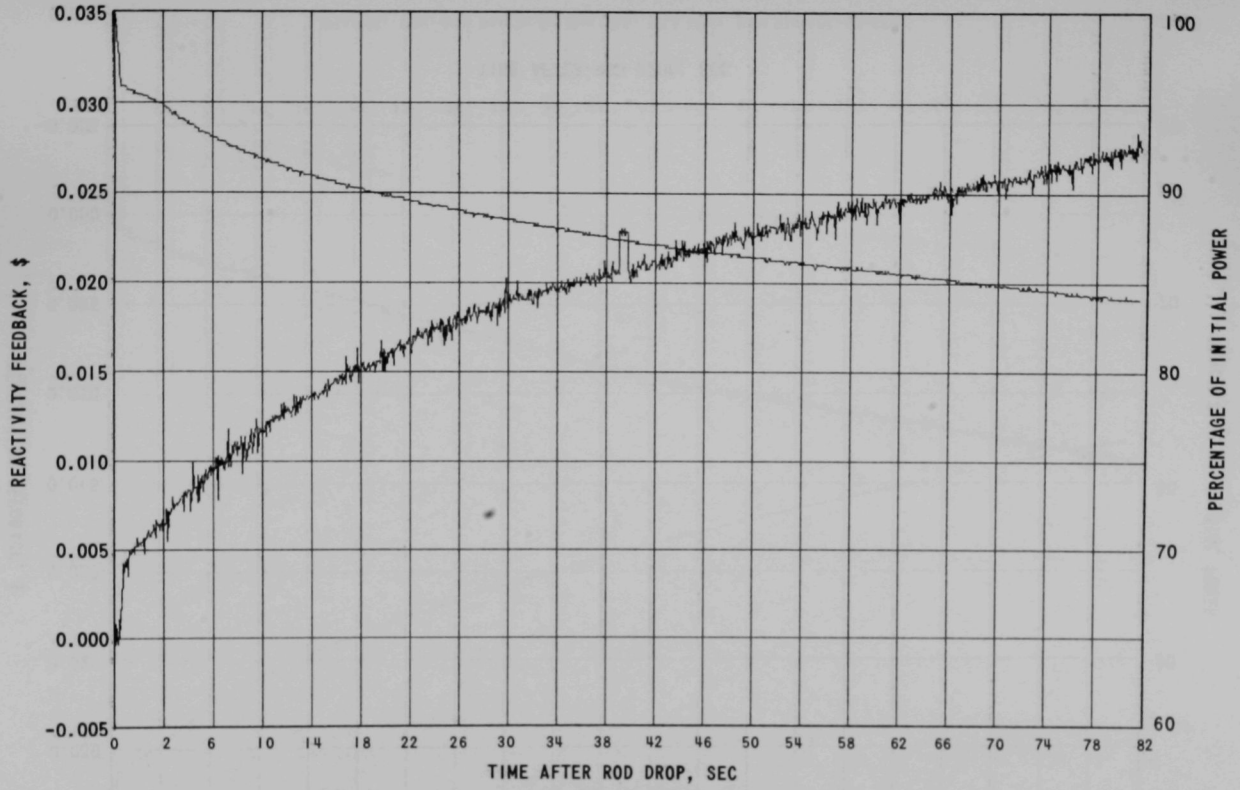

Fig. 47. Rod-drop Results for Run 29C, 22.5 MWt, 58% Flow (7-19-68)

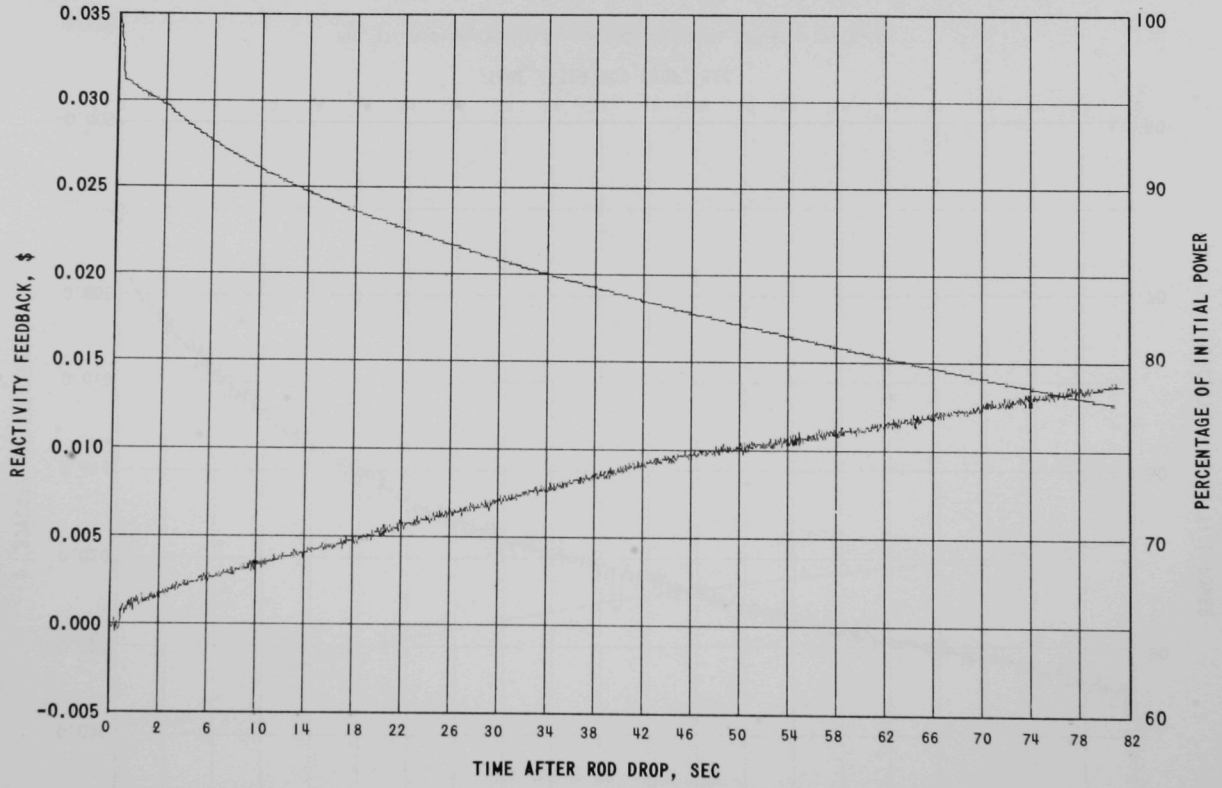

Fig. 48. Rod-drop Results for Run 30A, 12.5 MWt, Full Flow (8-27-68)

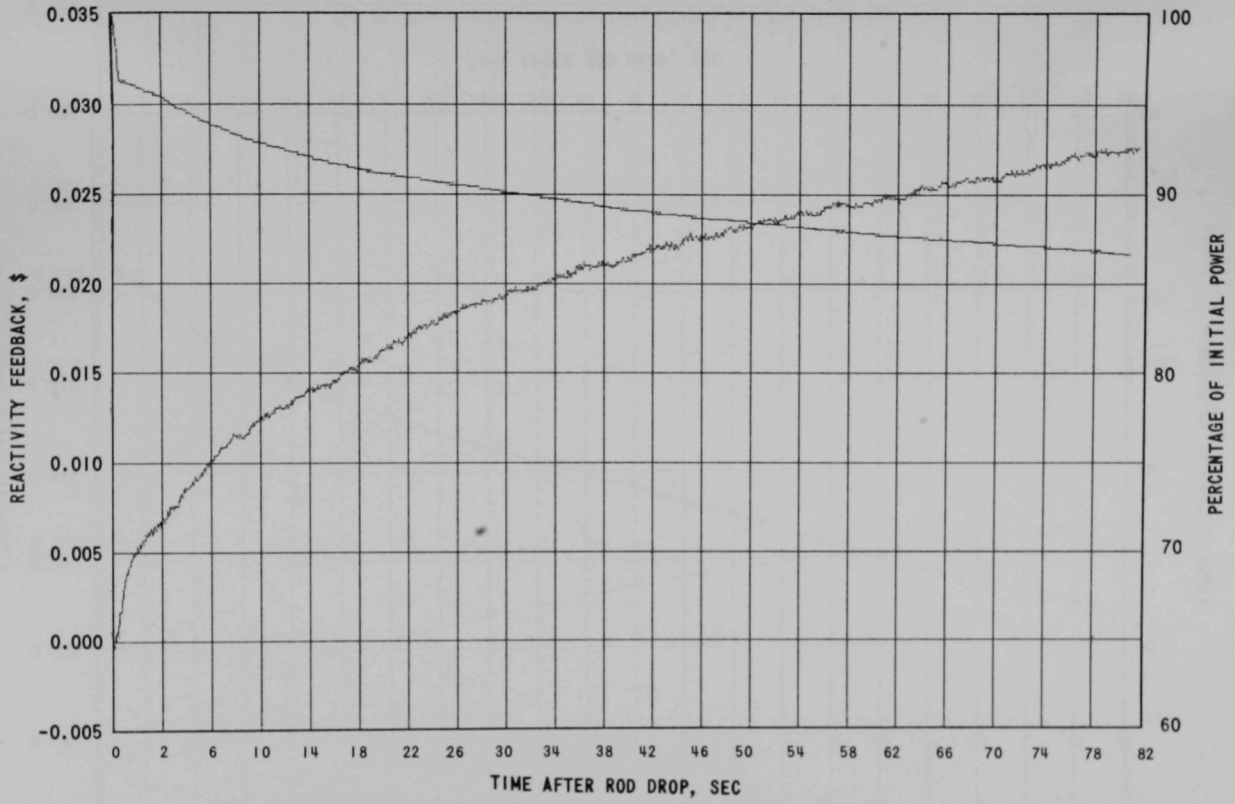

Fig. 49. Rod-drop Results for Run 30A, 41.5 MWt, Full Flow (8-27-68)

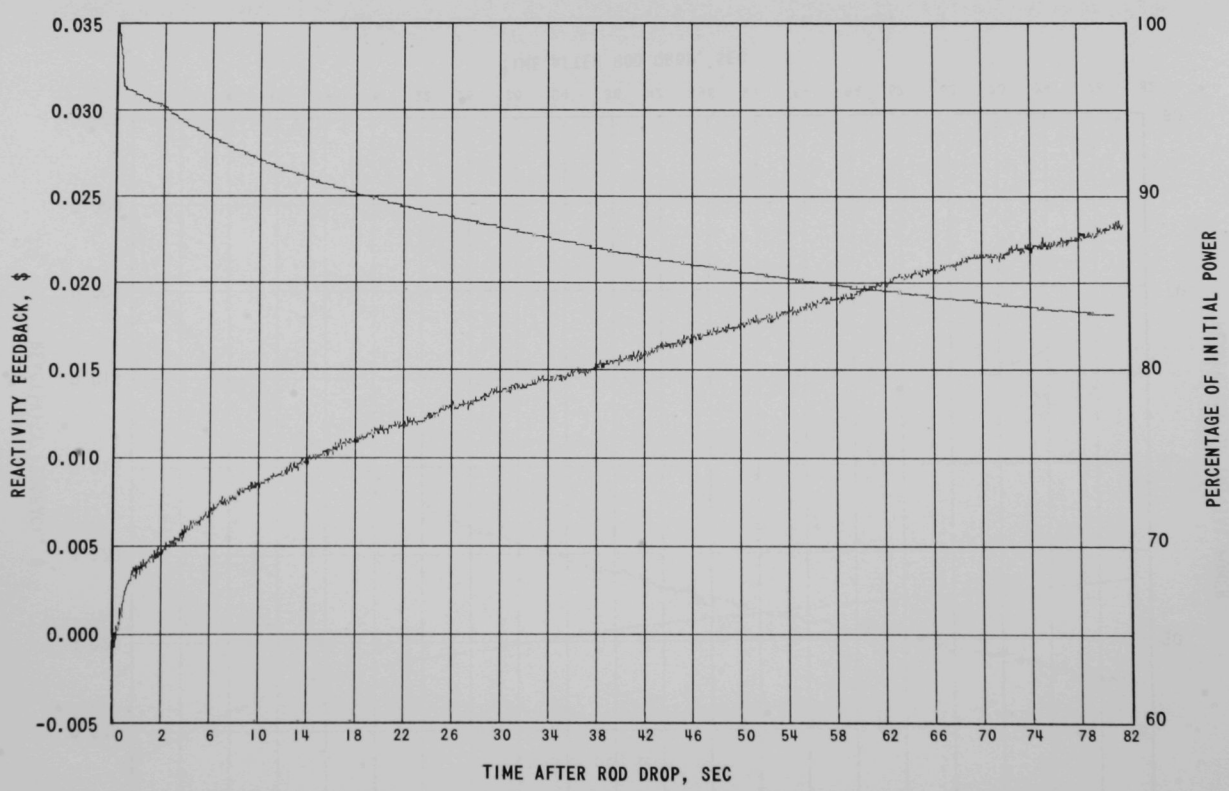

Fig. 50. Rod-drop Results for Run 30A, 25 MWt, Full Flow (8-27-68)

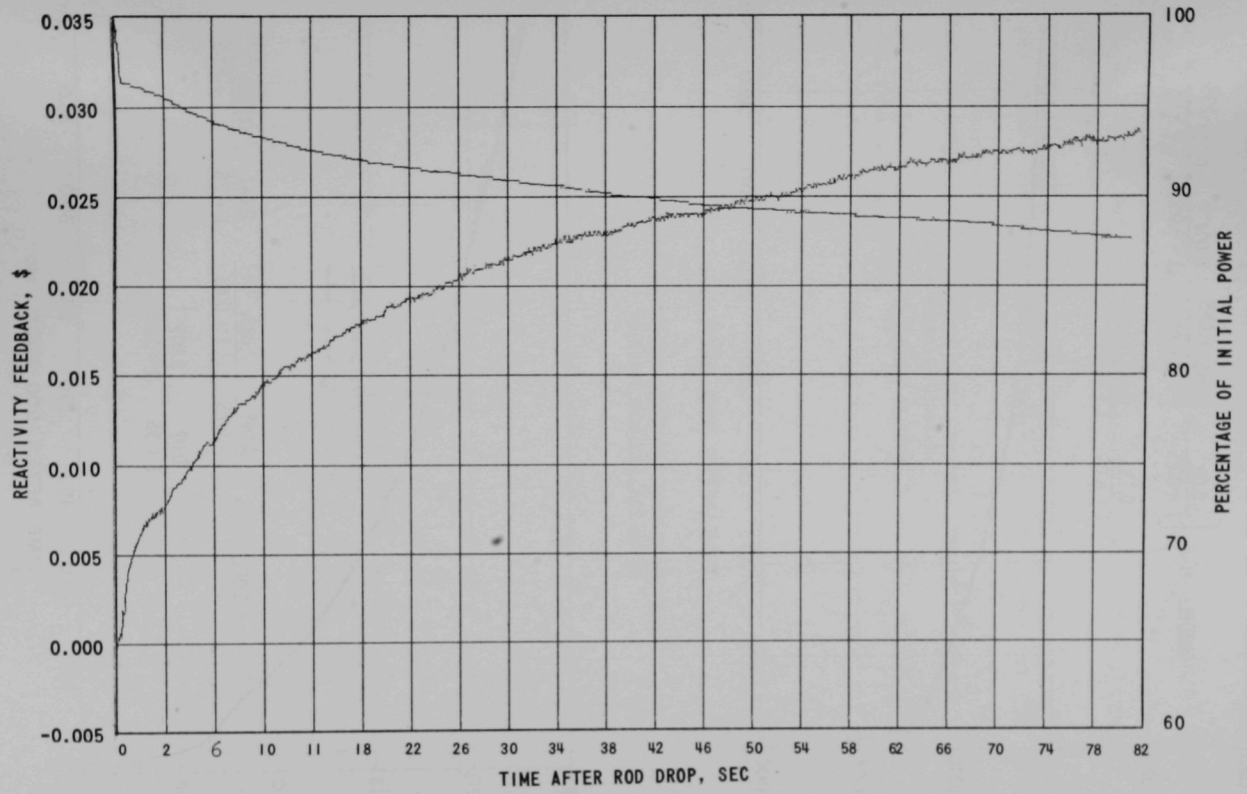

Fig. 51. Rod-drop Results for Run 30A, 50.0 MWt, Full Flow (8-27-68)

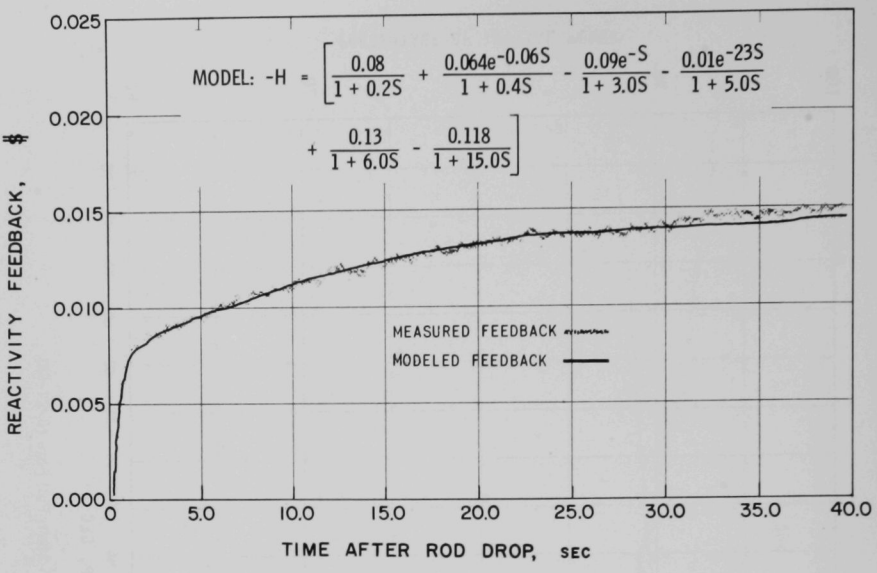

Fig. 52. Comparison of Measured and Modeled Feedback for Run 29A, 41.5 MWt, Full Flow

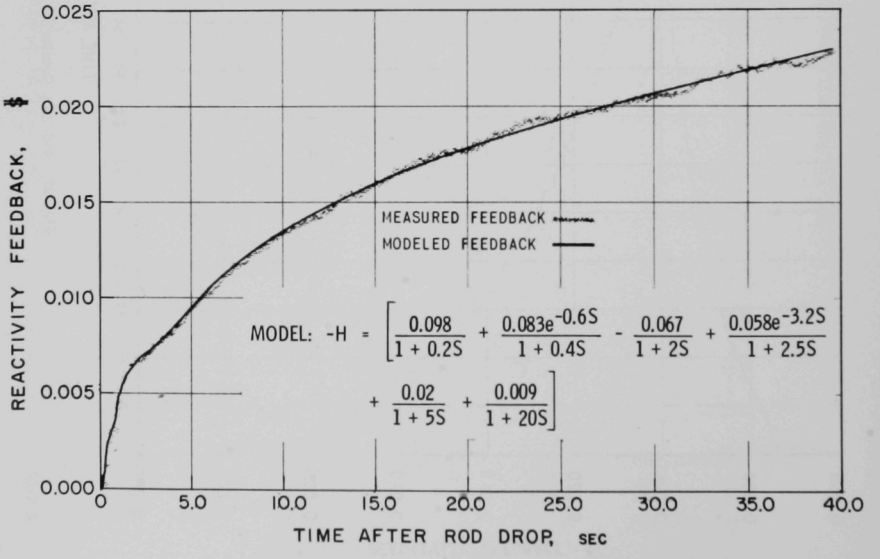

Fig. 53. Comparison of Measured and Modeled Feedback for Run 29C, 41.5 MWt, Full Flow

REFERENCES

1. R. W. Hyndman and M. R. Tuck, *An On-line Method of Transfer Function Analysis in EBR-II*, Nucl. Appl. *6*(2), 137-141 (1969).

2. R. W. Hyndman and R. B. Nicholson, *The EBR-II Feedback Function*, ANL-7476 (July 1968).

3. J. K. Long and W. R. Wallin, *A Documentation of Criticality Data for EBR-II with a Stainless Steel Radial Reflector*, ANL-7541 (Apr 1970).

4. M. A. Schultz, *Control of Nuclear Reactions and Power Plants*, 2nd Edition, p. 109, McGraw-Hill Book Co., New York (1961).

5. J. C. Case, *Core-loading Diagrams for EBR-II Runs 4 through 38*, ANL/EBR-007 (Dec 1969).